Biofilm formation and extracellular polymeric substances of acidophilic metal/sulfur-oxidizing archaea

Dissertation

zur Erlangung des akademischen Grades eines
Doktors der Naturwissenschaften
ïDr. rer. nat. ï

vorgelegt von

Ruiyong Zhang

geboren in Kaifeng, China

Biofilm Centre, Fakultät für Chemie
der
Universität Duisburg-Essen

2015

Die vorliegende Arbeit wurde im Zeitraum von Januar 2011 bis Januar 2015 im Arbeitskreis von Prof. Dr. W. Sand in der Fakultät für Chemie, Biofilm Center der Universität Duisburg-Essen durchgeführt.

Tag der Disputation: 22.12.2015

Gutachter: Prof. Dr. Wolfgang Sand

Prof. Dr. Thomas R. Neu

Vorsitzender: Prof. Dr. Jochen S. Gutmann

Thought is impossible without an ima

Aristotle (38382BC)

The results obtained during the promotion are partly in the following original publications published or in press:

Zhang R, Vera M, Bellenberg S, Sand W (2013) Attachment to minerals and biofilm development of extremely acidophilic archaea. Adv Mat Res 825:103-106

Zhang R, Bellenberg S, Castro L, Neu TR, Sand W, Vera M (2014) Colonization and biofilm formation of the extremely acidophilic archaeon *Ferroplasma acidiphilum*. Hydrometallurgy 150:245-252

Zhang R, Neu T, Bellenberg S, Kuhlicke U, Sand W, Vera M (2015) Use of lectins to in situ visualize glycoconjugates of extracellular polymeric substances in acidophilic archaeal biofilms. Microb Biotechnol 8:448-461

Zhang R, Neu T, Zhang Y, Bellenberg S, Kuhlicke U, Li Q, Sand W, Vera M (2015) Visualization and analysis of EPS glycoconjugates of the thermo-acidophilic archaeon *Sulfolobus metallicus*. Appl Microbiol Biotechnol 99:7343-7356

Zhang R, Zhang Y, Neu TR, Li Q, Bellenberg S, Sand W, Vera M (2015) Initial attachment and biofilm formation of a novel crenarchaeote on mineral sulfides. Adv Mat Res 1130:127-130

Zhang R, Liu J, Neu TR, Li Q, Bellenberg S, Sand W, Vera M (2015). Interspecies interactions of metal-oxidizing thermo-acidophilic archaea *Acidianus* and *Sulfolobus*. Adv Mat Res 1130:105-108

Zhang R, Bellenberg S, Neu TR, Sand W, Vera M (2016) The biofilm lifestyle of acidophilic metal/sulfur-oxidizing microorganisms. In: Rampelotto PH (ed) Biotechnology of Extremophiles: Advances and Challenges. Springer, Switzerland

Contents

Contents I

List of Abbreviations III

Abstract V

1. Introduction ..... - 1 -

1.1 State of art of bioleaching/biomining ..... - 1 -

1.2 Bioleaching mechanisms ..... - 2 -

1.3 Pathways of metal sulfide dissolution ..... - 3 -

1.4 Biodiversity of acidophilic microorganisms ..... - 5 -

1.4.1 The genus *Ferroplasma* ..... - 11 -

1.4.2 The genus *Acidianus* ..... - 13 -

1.4.3 The genus *Sulfolobus* ..... - 15 -

1.5 Attachment, EPS and biofilm of acidophiles ..... - 16 -

1.5.1 Attachment of acidophiles to surfaces ..... - 18 -

1.5.2 Biofilms of acidophiles ..... - 19 -

1.5.3 Extracellular polymeric substances of acidophiles ..... - 22 -

1.6 Analytical techniques for biofilm and EPS study ..... - 26 -

1.6.1 Atomic force microscopy ..... - 26 -

1.6.2 Confocal laser scanning microscopy and Epifluorescence microscopy ..... - 27 -

1.6.3 Fluorescence lectin-binding analysis ..... - 29 -

1.6.4 Fourier transform infrared spectroscopy ..... - 31 -

2. Aims of the Study ..... - 33 -

3. Materials and Methods ..... - 34 -

3.1 Strains and cultivation ..... - 34 -

3.2 Substratum, biofilm formation and pyrite leaching ..... - 34 -

3.3 Cell number, pH and iron determination ..... - 36 -

3.4 EPS extraction and chemical analysis ..... - 36 -

3.5 Staining ..... - 37 -

3.6 Fluorescence lectin-binding assays ..... - 37 -

3.7 Confocal laser scanning microscopy ..... - 38 -

3.8 Atomic force microscopy and Epifluorescence microscopy ..... - 39 -

3.9 Fourier transform infrared spectroscopy ..... - 39 -

3.10 Digital image analysis ..... - 40 -

4. Results and Discussion ..... - 41 -

4.1 Biofilm formation by the extremely acidophilic archaeon *F. acidiphilum* ..... - 41 -

4.2 Visualization of acidophilic archaeal biofilms on pyrite and S^0 ..... - 51 -

4.3 EPS analysis of the thermoacidophilic archaeon *S. metallicus* ..... - 74 -

5. Summary and Conclusions ..... - 100 -

6. Outlook ..... - 102 -

7. References ..... - 104 -

Acknowledgements ..... - 130 -

Curriculum Vitae ..... - 132 -

List of Publications ..... - 135 -

Deklaration ..... - 138 -

List of Abbreviations

AFM	Atomic force microscopy
AHLs	N-acyl homoserine lactones
AMD	acid mine drainage
ARD	acid rock drainage
ATR-FTIR	Attenuated Total Reflection-Fourier Transmission Infra-Red spectroscopy
BRGM	Bureau de Recherches Géologiques et Minières
BSA	bovine serum albumin
CLSM	Confocal laser scanning microscopy
Con A	Concanavalin A
DAPI	4´,6-diamidino-2-phenylindole
DDAO	7-hydroxy-9H-1,3-dichloro-9,9-dimethylacridin-2-one
DSMZ	Deutsche Stammsammlung von Mikroorganismen und Zellkulturen
eDNA	extracellular DNA
EFM	Epifluorescence microscopy
EPS	Extracellular polymeric substances
FITC	Fluorescein isothiocyanate
FLBA	Fluorescence lectin-binding analysis
G6PDH	Glucose-6-phosphate-dehydrogenase

GalNAc	N-acetylgalactosamine
GlcNAc	N-acetylglucosamine
HPLC	High-performance liquid chromatography
KDO	3-deoxy-D-manno-octulosonic acid
LPA	*Limulus polyphemus* agglutinin
MAC	Mackintosh basal salt medium
MIC	Minimum inhibitory concentration
MIP	Maximum intensity projection
MS	Metal sulfides
NA	Numerical aperture
QS	Quorum sensing
RISCs	Reduced inorganic sulfur compounds
ROS	Reactive oxygen species
SEM	Scanning electron microscopy
STXM	Scanning transmission X-ray microscopy
TRITC	Tetramethylrhodamine isothiocyanate
S-layer	Surface-layer
SOR	Sulfur oxygenase reductase
SQR	Sulfide:quinone oxidoreductase
µ-XRF	Micro X-ray fluorescence

Abstract

In this study, biofilm formation and extracellular polymeric substances (EPS) of acidophilic archaea were investigated. Three representative archaeal species extremely acidophilic archaeon *Ferroplasma acidiphilum*, thermoacidophilic archaea *Acidianus* sp. DSM 29099 and *Sulfolobus metallicus* were chosen as test organisms. Several cultivation and advanced microscopical techniques e.g. CLSM, AFM & EFM and SEM were used to visualize and characterize biofilm development and EPS of acidophilic archaea. In addition, FLBA, ATR-FTIR and conventional spectroscopic methods were applied for qualification and quantification of EPS components.

F. acidiphilum biofilms were heterogeneously distributed on polycarbonate filters over time, and varied within the different growth conditions such as supplementation with glucose. Cells formed a monolayer biofilm and were preferably attached to the defect sites of pyrite surfaces. Biofilm and planktonic cells exhibited significant morphological differences as revealed by AFM. Low coverage of pyrite surface by cells seems to correlate with their low leaching ability.

Screening of a lectin library resulted in the detection of 21 lectins able to bind archaeal biofilms on pyrite and to *Acidianus* sp. DSM 29099 biofilms on elemental sulfur (S^0). These lectins can be used in studies for assessment of interactions between various members of microbial bioleaching communities, especially in order to elucidate the role of archaea in detail. The major binding patterns, e.g. tightly bound EPS and loosely bound EPS, were detected on both substrates pyrite and S^0. The three archaeal species produced various EPS glycoconjugates containing sugar moieties like glucose, galactose, mannose, GlcNAc, GalNAc, sialic acid, and fucose. Additionally, the substratum induced

different EPS glycoconjugates and biofilm structures for cells of *Acidianus* sp. DSM 29099.

EPS analysis of *S. metallicus*^{T} on S^0 showed that capsular EPS from planktonic cells were mainly composed of carbohydrates and proteins. In contrast, colloidal EPS from planktonic cells were dominated by carbohydrates. Proteins were found to be major components in EPS from biofilms on S^0. In addition, extracellular proteins and nucleic acids were present in the EPS matrix. The existence of these compounds suggest their potential roles in biofilm formation and stabilization. *S. metallicus*^{T} cells were shown to be embedded in a gel-like and flexible EPS matrix, where cells were often found to be motile (back and forth) either self-propelled by cellular appendages or by Brownian mot

1. Introduction

1.1 State of art of bioleaching/biomining

Around 166 A. D., the medical doctor Galenus reported that blue copper sulfate containing water was extracted from copper mines on Cyprus (Rossi 1990). Since then the capacity of microbes to dissolve sulfide minerals has been explored for the last millennia. The process that metal sulfides (MS) are dissolved into bulk solutions under the effects of microorganisms is called bioleaching (Vera et al. 2013b; Schippers et al. 2014). On the one hand, bioleaching can be used for valuable metal recovery from ore deposits and concentrates. On the other hand, bioleaching may cause acidification of water resources, leading to serious environment pollution like acid mine/rock drainage (AMD/ARD) (Sand et al. 2007; Hallberg 2010; Nordstrom et al. 2015).

Biomining is the term to describe the technology that uses microbes to achieve metal extraction from minerals or waste materials. Biomining of gold or other precious metals normally involves a pre-treatment process using metal/sulfur-oxidizing bacteria or archaea prior to cyanide extraction (Syed 2012). This process is known as biooxidation. Compared to the traditional mineral processing technology like ore smelting/toasting, biomining is more attractive regarding to its lower energy costs and also is more environmentally friendly. In addition, due to the autotrophic lifestyle of most bioleaching microbes, CO_2 is fixed by during their bio-processing of MS. This means that bioleaching involves less carbon footprints (CO_2 fixation by autotrophs) compared to smelting operations (CO_2 emission) (Johnson 2014).

Normally, MS dissolution is a metal oxidation process due to the presence of reduced metal ions in MS. Some oxide ores can be leached by a bioreductive leaching, a process (due Pass is et called al. 2011) ed ñ Ferredoxò

It is assumed that 15 % of copper, 5 % of gold and smaller amounts of other metals (such as nickel and zinc) are currently produced globally using

biomining technologies. Apart from base metals like copper and nickel, precious metals like gold, uranium, and rare-earth elements have also been exploited from underground ore bodies *in situ* (Johnson 2015).

Biomining is also applied to recover valuable metals from electrical-electronic wastes (Pant et al. 2012; Hong and Valix 2014), spent petroleum and fly ash (Akcil et al. 2015), oxide ores (i.e. lateritic ores) (Johnson et al. 2013; Nancucheo et al. 2014), process waters and water streams (Johnson 2013). In addition, biomining has been actively studied over the last several years as a bioremediation tool for treating heavy metals contained in sewage sludge, sediment, and contaminated soil and mine tailings (Liu et al. 2007; Lim et al. 2009; Pathak et al. 2009; Deng et al. 2013; Lee et al. 2015).

Modern "Omics" tools, such as genomics, proteomics, transcriptomics and metabolomics have been used to elucidate diversity and some ecological aspects of acidophilic communities, bioleaching mechanisms, and will be helpful in future attempts to optimize the design, control, and optimization of bioleaching applications (Vera et al. 2013a; Goltsman et al. 2015; Martinez et al. 2015). Increased standards for environmental protection and the demand of base and precious metals as well as rare-earth elements will definitely intensify the use of bio-processing of ore minerals.

1.2 Bioleaching mechanisms

The mechanisms involved in mineral dissolution conducted by microorganisms have been debated for decades (Evangelou and Zhang 1995; Bosecker 1997; Tributsch 2001; Crundwell 2003). Microbial dissolution of minerals has been postulated to be a result of direct and indirect leaching mechanisms. However, it is now well accepted that the originally dis (assuming that the cells are able to enzymatically oxidize the sulfur moiety at the MS surface) does not exist (Sand et al. 2001). The indirect mechanism consists two sub-mechanisms: contact and non-contact mechanisms. In case of

the contact mechanism, cells attach to and form biofilms on MS via extracellular polymeric substances (EPS) and consequently enhance mineral degradation. In the non-contact mechanism, microorganisms in the planktonic phase are responsible for regeneration of iron(III) ions which attack the MS and lead to its dissolution (Sand et al. 2001; Rawlings 2002). As a result, a combined mechanism in which both cell subpopulations (i.e. biofilm forming cells on the MS and planktonic cells contribute to MS dissolution by providing iron(III) ions and/or protons thanks to their iron/sulfur oxidation activities (Vera et al. 2013b).

1.3 Pathways of metal sulfide dissolution

Based on the acid solubility of MS, there are two different pathways of mineral dissolution (Fig. 1). The thiosulfate pathway is involved in the dissolution of acid-insoluble MS, such as pyrite, molybdenite (MoS_2), and tungstenite (WS_2). The polysulfide pathway is relevant for dissolution of acid-soluble MS, such as sphalerite (ZnS), galena (PbS) or chalcopyrite (Schippers et al. 1996; Schippers and Sand 1999; Sand et al. 2001).

These two pathways are indirect mechanisms, since in acidic solution the acid-insoluble MS are solely oxidized chemically by iron(III) ions, which are supplied by the microbial oxidation of iron(II) ions (Schippers et al. 1996; Rodriguez et al. 2003; Gleisner et al. 2006). The electrochemical processes that result in the dissolution of sulfide minerals take place at the interface between the bacterial cell and the mineral sulfide surface.

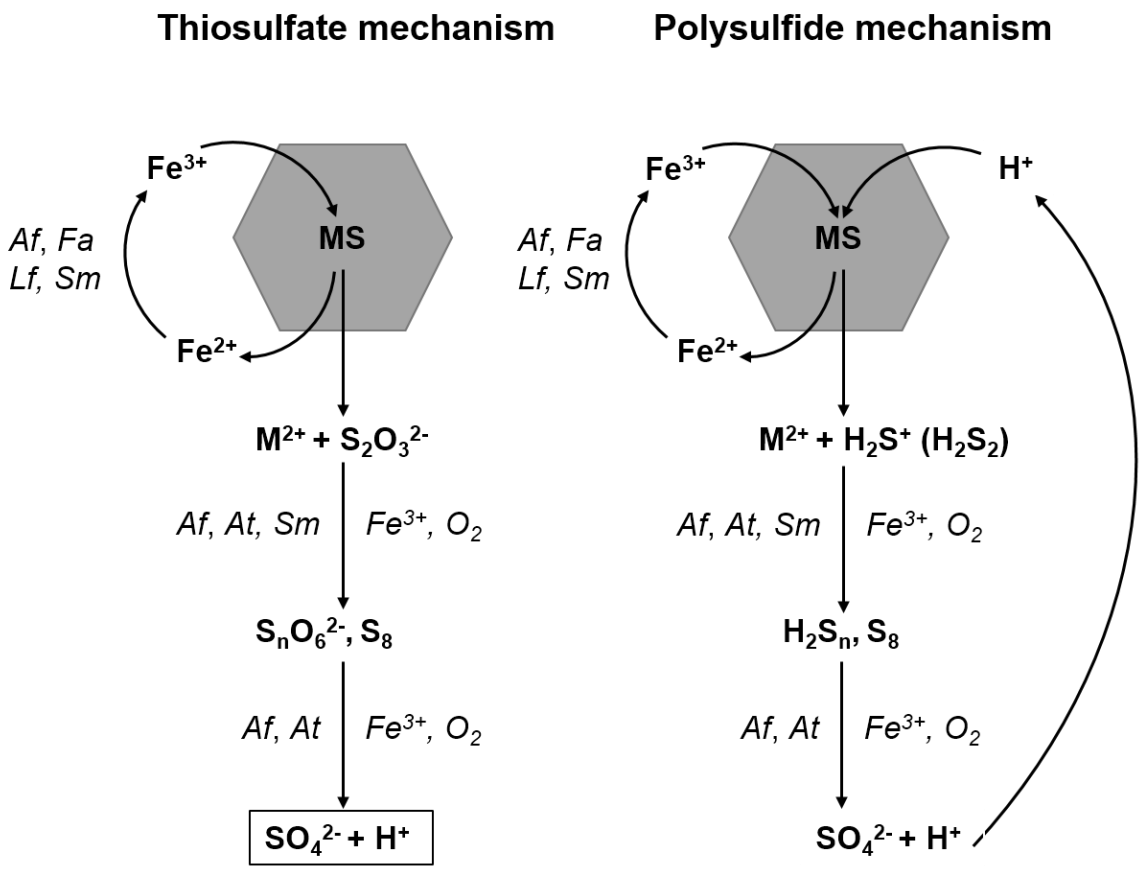

Figure 1. Scheme of the thiosulfate and polysulfide mechanisms in the bioleaching of MS (modified from Schippers and Sand 1999). Iron(III) ions attack MS by electron extraction and are thereby reduced to the iron(II) ion form. As a result, the metal sulfide crystal releases metal cations (M^{2+}) and water-soluble intermediary sulfur compounds. Iron(II)-oxidizing bacteria and archaea such as *Acidithiobacillus ferrooxidans* (*Af*), *Ferroplasma acidiphilum* (*Fa*), *Leptospirillum ferrooxidans* (*Lf*), and *Sulfolobus metallicus* (*Sm*) catalyze the recycling of iron(III) ions in acidic solutions.

For the case of pyrite the anodic and cathodic reactions have been reviewed. In the first step, a cathodic reaction transfers electrons from the surface of the pyrite (cathode) to the aqueous oxidant species, usually O_2 or iron(III) ions. The second step transports charge (electrons) from the site of an anodic reaction to replace the electron lost from the cathodic site. In the third step, at an anodic site, the oxygen atom of a water molecule interacts with a sulfur atom to create

a sulfoxy species. This releases an electron into the pyrite and one or two hydrogen ions to the bulk solution. These three steps occur more or less simultaneously in the actual oxidation process (Rimstidt 2003). These anodes and cathodes may be resulting from imperfections in the crystal lattice where the iron to sulfur ratio is imbalanced due to inclusion of other metal atoms during the process of crystallization and/or from variations of temperature during crystallization (causing amorphous up to highly crystalline structures).

1.4 Biodiversity of acidophilic microorganisms

Bioleaching of MS is performed by a diverse group of microorganisms (Schippers 2007; Schippers et al. 2010). Several species have been identified in bioleaching operations and AMD environments (Johnson 1998; Schippers 2007; Méndez-García et al. 2015). Leaching bacteria are distributed among the *Proteobacteria* (*Acidithiobacillus*, *Acidiphilium*, *Acidiferrobacter*, *Ferrovum*), *Nitrospirae* (*Leptospirillum*), *Firmicutes* (*Alicyclobacillus*, *Sulfobacillus*) and *Actinobacteria* (*Ferrimicrobium*, *Acidimicrobium*, *Ferrithrix*). Few fungal species like *Phanerochaete chrysosporium*, *Aspergillus niger* and *Penicillium citrinum* have been reported in bio-oxidation of gold-bearing ores or metal recovery (Acharya et al. 2002; Ofori-Sarpong et al. 2013; Yang et al. 2013). The most studied acidophilic archaea generally include the order *Thermoplasmatales* and *Sulfolobales*. To date, the only known extreme thermoacidophiles belong to the crenarchaeotal class of *Thermoprotei*, represented by the orders *Desulfurococcales*, *Thermoproteales*, *Fervidococcales*, *Acidilobales*, and *Sulfolobales*. The order *Sulfolobales* is comprised of the genera *Sulfolobus*, *Acidianus*, *Metallosphaera*, *Sulfurococcus*, *Stygioglobus*, and *Sulfurisphaera*. Only several species from the order *Sulfolobales* like *Acidianus*, *Sulfolobus* and *Metallosphaera* have been reported to be relevant for bioleaching applications (Norris 2007; Auernik et al. 2008; Pradhan et al. 2008; Wheaton et al. 2015).

The Euryarchaeota order *Thermoplasmatales*, which grow at mesophilic or moderately thermophilic conditions, are also often found in bioleaching and AMD systems (Golyshina and Timmis 2005; Golyshina 2011). The general physiology of members of *Sulfolobales* and *Thermoplasmatales* is presented in Table 1. Among those, the phylogenetic relationships of the main bacterial and archaeal species involved in bioleaching are illustrated in Fig. 2.

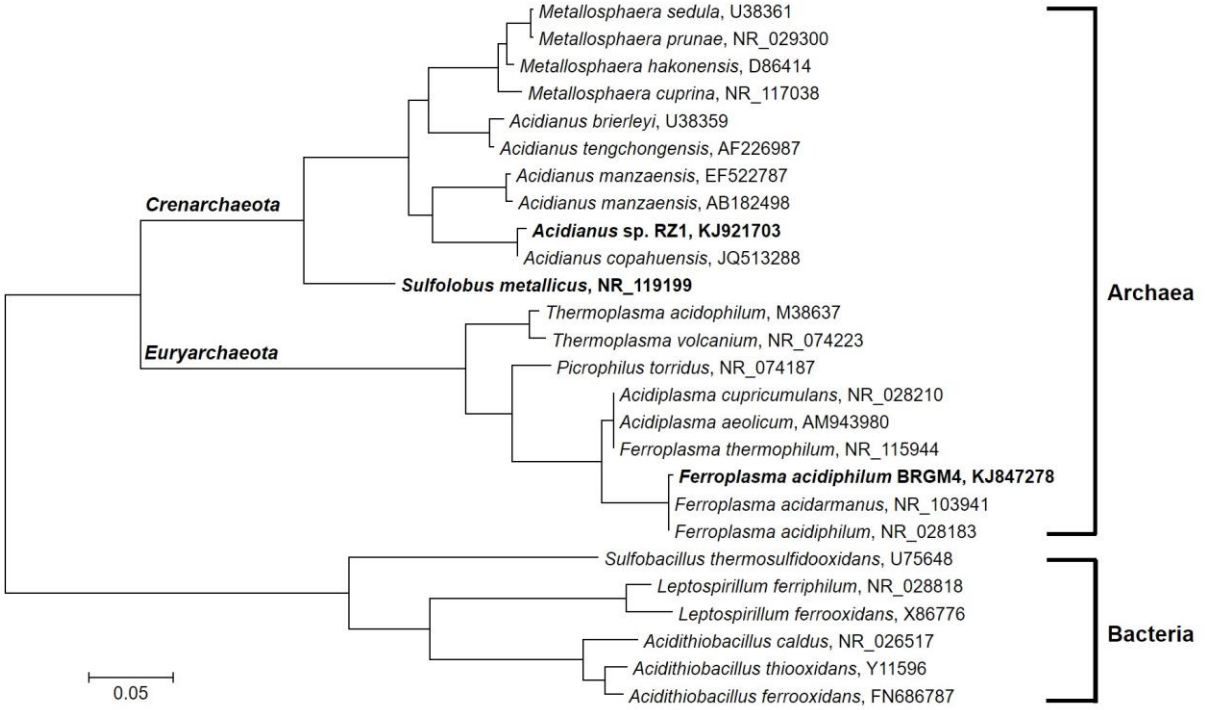

Figure 2. Phylogenetic tree showing affiliations of acidophilic archaea and bacteria based on their 16S rRNA sequences. The GenBank accession number downloaded from NCBI database is shown after each species. The three archaeal species used in the current study are shown in bold. The scale bar represents of 5 % sequence divergence. MEGA 6 was used to construct the maximum-likelihood (ML) phylogenetic tree (Tamura et al. 2013).

Table 1. Characteristics of the acidophilic archaea *Thermoplasmales* and *Sulfolobales*. CW: cell wall. A: Aerobic. FA: Facultative anaerobic. COC: complex organic compounds. Opt.: Optimum. T°: Temperature (°C).

Species	**Origin**	**Cell shape**	**CW**	**Relation to O_2**	**Energy substrates**	**Growth T°**		**Growth pH**		**Growth modes**	**References**
						Opt.	**Range**	**Opt.**	**Range**		
Thermoplasma acidophilum (DSM1728^T)	Coal refuse pile, Indiana	Cocci	-	FA	COC, sugars	59	45-63	1-2	0.5-4	Heterotrophic	(Darland et al. 1970; Segerer et al. 1988)
Thermoplasma volcanium (DSM 4299^T)	Acid solfatara Vulcano, Italy	Irregular cocci	-	FA	COC, sugars	60	33-67	2	1-4	Heterotrophic	(Segerer et al. 1988)
Picrophilus oshimae (DSM 9789^T)	Solfatara, Hokkaido, Japan	Irregular cocci	+	Aerobic	COC, sugars	60	47-65	0.7	0-3.5	Heterotrophic	(Schleper et al. 1995)
Picrophilus torridus (DSM 9790^T)	Solfataric field Hokkaido, Japan	Irregular cocci	+	Aerobic	COC, sugars	60	47-65	0.7	0-3.5	Heterotrophic	(Schleper et al. 1995)
Ferroplasma acidiphilum (DSM 12658^T)	Bioreactor for arsenopyrite Kazakhstan	Pleomorphic	-	FA	Fe^{2+}, sulfide ores, COC, sugars	37	15-45	1.7	1.3-2.2	Mixtrophic	(Golyshina et al. 2000)
Ferroplasma acidarmanus (Fer 1)	Iron Mountain, California	Pleomorphic Irregular cocci	-	FA	Fe^{2+}, sulfide ores, COC, sugars	42	23-46	1.2	’0.2-2.5	Mixtrophic	(Edwards et al. 2000b; Dopson et al. 2004)
Ferroplasma thermophilum (L1)	Daye Copper mine, China	Cocci	-	FA	Fe^{2+}, sulfide ores, COC, sugars	45	30-60	1	0.2-2.5	Mixtrophic	(Zhou et al. 2008)

Thermogymnomonas acidicola (DSM 18835^T)	Solfataric field Hakone, Japan	Pleomorphic	-	Aerobic	COC, sugars	60	38-68	3	1.8-4	Heterotrophic	(Itoh et al. 2007)
Acidiplamsa cupricumulans (DSM 16551^T)	Chalcocite heaps, Myanmar	Irregular cocci	-	FA	Fe^{2+}, sulfide ores, COC, sugars	53.6	22-63	1-1.2	0.4-1.8	Mixtrophic	(Hawkes et al. 2006; Golyshina et al. 2009)
Acidiplasma aeolicum (DSM 18409^T)	Hydrothermal pool, Vulcano	Pleomorphic Irregular cocci	-	FA	Fe^{2+}, sulfide ores, COC, sugars	45	15-65	1.4-1.6	0-4	Mixtrophic	(Golyshina et al. 2009)
Sulfolobus acidocaldarius (DSM 639^T)	Hot spring, Yellowstone National Park	Irregular lobed	+	Aerobic	COC, sugars	70-75	55-85	2-3	1-5.9	Heterotrophic	(Brock et al. 1972)
Sulfolobus solfataricus (DSM 1616^T)	Hot spring, Pisciarelli Solfatara, Italy	Spherical irregular polyhedrons	+	Aerobic	COC, sugars	80	65-87	3	2-4	Heterotrophic	(Zillig et al. 1980)
Sulfolobus shibatae (DSM 5389^T)	Geothermal pool, Kiushu Island, Japan	Irregular cocci	+	Aerobic	COC, sugars, S^0	81	ND-86	3	ND	Heterotrophic	(Grogan et al. 1990)
Sulfolobus metallicus (DSM 6482^T)	Solfataric fields, Iceland	Irregular lobed cocci	+	Aerobic	Fe^{2+}, sulfide ores, S^0, $K_2S_4O_6$	65	50-75	ND	1-4.5	Autotrophic	(Huber and Stetter 1991)
Sulfolobus rivotincti	Rio Tinto Huelva, Spain	ND	ND	Aerobic	Fe^{2+}, sulfide ores	68.5	ND	ND	ND	Autotrophic	(Gómez et al. 1999)
Sulfolobus yangmingensis (YM1^T)	Yang-Ming National Park, Taiwan	Lobed	ND	Aerobic	COC, sulfide ores, sugars, S^0, $K_2S_4O_6$	80	65-95	4	2-6	Autotrophic or mixtrophic	(Jan et al. 1999)
Sulfolobus tokodaii (DSM 16993^T)	Hot Springs, Kyushu Island, Japan	Irregular cocci	+	Aerobic	COC, sugars, S^0	80	70-85	2.5-3	2-5	Mixtrophic	(Suzuki et al. 2002)

Sulfolobus tengchongensis (RT8-4^T)	Hot spring, Tengchong, China	Irregular cocci	ND	Aerobic	COC, sugars, S^0	85	65-95	3.5	1.7-6.5	Mixtrophic	(Xiang et al. 2003)
Acidianus brierleyi (DSM 1651^T)	Hot spring, Yellowstone National Park	Spherical, irregular polyhedrons	+	FA	Fe^{2+}, sulfide ores, COC, sugars, S^0	70	45-75	1.5-2	1-6	Autotrophic or heterotrophic	(Zillig et al. 1980; Segerer et al. 1986)
Acidianus infernus (DSM 3191^T)	Solfatara Crater, Naples, Italy	Irregular cocci	+	FA	H_2S, S^0	90	65-96	2	1-5.5	Autotrophic	(Segerer et al. 1986)
Acidianus ambivalens (DSM 3772^T)	Solfatara, Iceland	Irregular lobed cocci	+	FA	H_2S, S^0	80	70-87	2.5	1-3.5	Autotrophic	(Zillig et al. 1986; Fuchs et al. 1996)
Acidianus tengchongensis (AS 1.3347^T)	Hot spring, Tengchong, China	Irregular cocci	ND	FA	S^0, $S_2O_3^{2-}$	70	60-75	1.5-2	1-5.5	Autotrophic	(He et al. 2004)
Acidianus manzaensis (NBRC 100595^T)	Fumarole in Manza, Japan	Cocci	+	FA	S^0, COC, sugars	80	60-90	1.0-5.0	1.2-1.5	Autotrophic or Mixtrophic	(Yoshida et al. 2006)
Acidianus sulfidivorans (DSM 18786^T)	Solfatara, Papua New Guinea	Irregular cocci	+	FA	S^0, Fe^{2+}, sulfide ores	74	45-83	0.8-1.4	0.35-3	Autotrophic or Mixtrophic	(Plumb et al. 2007)
Acidianus copahuensis (DSM 29038)	Copahue geothermals, Argentina	Irregular cocci	+	FA	S^0, Fe^{2+}, sulfide ores, sugars	75	55-80	2.5-3	1-5	Autotrophic or Mixtrophic	(Giaveno et al. 2013)
Metallosphaera sedula (DSM 5348^T)	Thermal pond in Pisciarelli Solfatara, Italy	Slightly irregular cocci	+	Aerobic	Fe^{2+}, S^0, $K_2S_4O_6$, sulfide ores, COC, sugars	75	50-80	2	1-4.5	Autotrophic or Mixtrophic	(Huber et al. 1989)
Metallosphaera prunae (DSM 10039^T)	Smoldering slag heap, Thüringen	Lobed cocci	+	FA	S^0, sulfide ores, COC, sugars	75	55-80	2	1-4.5	Autotrophic or Mixtrophic	(Fuchs et al. 1995)

Metallosphaera hakonensis (DSM 7519^T)	Geothermals, Hakone National Park	Lobed	+	Aerobic	H_2S, Fe^{2+}, S^0, $K_2S_4O_6$, $S_2O_3^{2-}$, sulfide ores, COC, sugars	70	50-80	3	1-4	Autotrophic or Mixtrophic	(Takayanagi et al. 1996; Kurosawa et al. 2003)
Metallosphaera yellowstonensis (MK1^T)	Acidic iron mat, Yellowstone National Park	Lobed cocci	+	Aerobic	Fe^{2+}, S^0, sulfide ores, COC	65-75	45-85	2-3	1-4.5	Autotrophic or Mixtrophic	(Kozubal et al. 2008)
Metallosphaera cuprina (Ar-4^T)	Hot spring, Tengchong	Irregular cocci	ND	Aerobic	Fe^{2+}, S^0, $K_2S_4O_6$, $S_2O_3^{2-}$, sulfide ores, COC, sugars	65	55-75	3.5	2.5-5.5	Autotrophic or Mixtrophic	(Liu et al. 2011)
Stygiolobus azoricus (DSM 6296^T)	Geothermals São Miguel Island	Highly irregular cocci	+	Anaerobic	H_2	80	57-89	2.5-3	1-5.5	Autotrophic or Mixtrophic	(Segerer et al. 1991)
Sulfurisphaera ohwakuensis (DSM 12421^T)	Hot spring Ohwaku Valley, Japan	Slightly irregular cocci	+	FA	S^0, COC	84	63-92	2	1-5	Mixtrophic	(Kurosawa et al. 1998)
Sulfurococcus yellowstonensis (Str6kar^T)	Thermal spring, Yellow Stone National Park	Spherical	+	Aerobic	Fe^{2+}, S^0, sulfide ores, COC, Sugars	60	40-80	2-2.6	1.0-5.5	Autotrophic or Mixtrophic	(Karavaiko and Lobyreva 1994; Karavaiko et al. 1994)
Sulfurococcus mirabilis (INMI AT-49^T)	Uzon volcano, Kamchatka, Russia	Spherical	+	Aerobic	S^0, sulfide ores, COC, sugars	70-75	50-86	2-2.6	1-5.8	Autotrophic or Mixtrophic	(Golovacheva et al. 1987; Karavaiko and Lobyreva 1994)

Note:

+: with CW. -: without CW. ND: not determined

Table modified from Wheaton et al. 2015

1.4.1 The genus *Ferroplasma*

The first *Ferroplasma* species *Ferroplasma acidiphilum* was isolated from a semi-industrial bioleaching pilot plant processing gold-containing arsenopyrite from Kazakhstan (Golyshina et al. 2000). Since then, two other recognized species *Ferroplasma acidarmanus* and *Ferroplasma thermophilum* and several isolates have been reported (Okibe et al. 2003; Dopson et al. 2004; Zhou et al. 2008; Bryan et al. 2009). *Ferroplasma* spp. can oxidize iron(II) ions, MS or organic compounds to sustain growth. Although genomic data showed that *Ferroplasma* spp. possess some genes encoding enzymes probably involved in hydrogen sulfide oxidation such as sulfide:quinone oxidoreductase (SQR) and elemental sulfur (S°) oxidation such as sulfur oxygenase reductase (SOR) (Jones et al. 2014; Janosch et al. 2015), sulfur oxidation by cells of *Ferroplasma* spp. has not been reported yet. All the isolated strains are capable of growing mixotrophically and aerobically, and most of them can also grow anaerobically (Dopson et al. 2004). Anaerobic growth of *Ferroplasma* spp. occurs by coupling oxidation of organic compounds with the reduction of iron(III). Sulfate, nitrate, sulfite, thiosulfate, and arsenate are not utilized as electron acceptors. Rates of iron(III) reduction by *Ferroplasma acidarmanus* fer1 are comparable with other acidophilic heterotrophs such as *Acidiphilium acidophilum* (Dopson et al. 2007).

Ferroplasma spp. are frequently detected in various acidic man-made operations like leaching tanks/heaps and also natural habitats like AMD sites, which are considered as hostile environments (Golyshina 2011; Méndez-García et al. 2015). They are considered to be major players in global iron and sulfur cycling (Edwards et al. 2000b; Golyshina and Timmis 2005). The family *Ferroplasmaceae* received scientific attention for its lifestyle in extremely acidic environments and provided new insights into acid and metal tolerance for cells without a protective cell wall. A key explanation for *Ferroplasma* spp. flourishing in acidic environments is their membrane lipids, which are mainly

composed of caldarchaetidylglycerol tetraether-linked monolayers (Macalady et al. 2004). All enzymes analyzed in *F. acidiphilum* were stable *in vitro* in the pH range of 1.7-4.0, and had pH optima much lower than their intracellular pH, estimated to be of ~5.6. This ó pHp t i m u m a n o m a l y ô s u g g e s yet-undetected cellular compartmentalization providing cytoplasmic pH patchiness and low pH environments for the analyzed enzymes (Golyshina et al. 2006). *F. acidiphilum* has a unique iron-protein-dominated cellular machinery. It has been shown that most of the investigated cellular proteins of *F. acidiphilum* are iron-metalloproteins. These include proteins with deduced structural, chaperone and catalytic roles, not described as iron-metalloproteins in any other organism so far investigated. The iron atoms in the proteins seem to organize and stabilize their 3-d i m e n s i o n a l s t r u c t u r e s , (Ferrer et al. 2007). *F. acidarmanus* has a minimum inhibitory concentration (MIC) for copper of 312 mM, which is lower than the value for *At. ferrooxidans* (800 mM) but higher than the one for *Sulfolobus metallicus* (200 mM) (Baker-Austin et al. 2005; Orell et al. 2010). It is the most metal (copper)-resistant archaeon to date. It has been shown that *F. acidarmanus* fer1 uses multiple mechanisms e.g. DNA repair and protein chaperones, for resistance against high levels of copper (Baker-Austin et al. 2005). Recently, two respiratory membrane protein complexes were characterized to be involved in iron oxidation respiratory chains, functioning in the uphill and downhill electron flow pathways (Castelle et al. 2015).

Cells of *Ferroplasma* usually promote the growth and metabolic activity of some other leaching bacteria by detoxifying leaching liquors and thus contributing to the maintenance of robust bioleaching microbial communities. Although pyrite leaching by *Leptospirillum ferriphilum* was depressed by *F. acidiphilum* (strain MT17), the inclusion of *Acidithiobacillus caldus* to the mixed cultures of *L. ferriphilum* and *F. acidiphilum* resulted in higher leaching efficiencies compared to pure cultures of *L. ferriphilum* (Okibe and Johnson

2004). Recently, a study also confirmed that the addition of *F. thermophilum* improved copper concentrate dissolution by *A. caldus* and *L. ferriphilum* (Zhang et al. 2015). A metabolic model was constructed for a mixed culture of *F. acidiphilum* and *L. ferriphilum*. This metabolic model, composed of 152 internal reactions and 29 transport reactions, describes the main interactions between these species, assuming that both use iron(II) ions as energy source, and *F. acidiphilum* takes advantage of the organic compounds secreted by *L. ferriphilum* for chemomixotrophic growth (Merino et al. 2014).

1.4.2 The genus *Acidianus*

All strains of *Acidianus* are thermophiles, facultative anaerobes and capable of chemolithoautotrophy and, in some instances, facultative autotrophy. Since the genus *Acidianus* was introduced in 1986 by Segerer and coworkers (1986), seven species have been described up to now (Table 1). The first species *A. brierleyi* was characterized previously as a member of the genus *Sulfolobus* and then re-classified as *Acidianus* (Zillig et al. 1980; Segerer et al. 1986). *A. brierleyi* has an irregular coccoid shape and cell sizes between 1 to 1.5 µm in diameter. It grows between 45 and 75 °C and pH 1 to 6. Its optimum growth, however, occurs at 70 °C and pH 1.5 to 2.0. It appears as yellow-orange under aerobic conditions and greyish-black under anaerobic ones (Segerer et al. 1986). One unique feature of *A. brierleyi* is its ability to live either chemoheterotrophically on yeast extract or chemolithoautotrophically (Larsson et al. 1990). These characteristics make *A. brierleyi* an ideal microorganism for bioleaching and one of the most frequently studied thermoacidophiles for bioleaching.

Although iron oxidation by *A. brierleyi* was shown to be slower than by the mesophile *At. ferrooxidans* (Nemati and Harrison 2000a), bioleaching of pyrite, chalcopyrite or sphalerite by *A. brierleyi* showed higher efficiencies compared to mesophiles (Konishi et al. 1995; Konishi et al. 2001). The presence of *A.*

brierleyi greatly accelerated the leaching of chalcopyrite concentrate (Konishi et al. 1999). This can be due to the fact that *A. brierleyi* possessing high sulfur oxidation activity, which can effectively remove passivating layers of S^0 accumulated on the mineral surface (Zhu et al. 2011; Liang et al. 2012). In addition, temperature effect is another reason because the rate of chemical reactions generally increases with an increase in temperature. Supplementary activated carbon or sodium chloride can accelerate the chalcopyrite dissolution by *A. brierleyi* (Liang et al. 2010; Liang et al. 2012). Yeast extract supplementation also increased the pyrite dissolution rate by *A. brierleyi* (Konishi et al. 1998). UV-induced mutants of *A. brierleyi* have been obtained with an improved bioleaching efficiency for MS (Meng et al. 2007).

A. brierleyi was found to be the dominant thermophile in a bioleaching community processing chalcopyrite concentrates (Dinkla et al. 2009). Recently, *A. brierleyi* was successfully used to leach spent catalyst: apart from removing volatile impurities and increasing the surface, cells could efficiently oxidize MS and achieved a high bioleaching of a coked catalyst. In addition, the importance of the non-contact mechanism in bioleaching of spent catalyst by *A. brierleyi* was highlighted (Bharadwaj and Ting 2013).

In the case of *A. manzaensis*, leaching of chalcopyrite was suggested to occur by the cooperative action of the contact and non-contact mechanisms (Zhang et al. 2010). Cells of *A. manzaensis* grown on solid substrates such as chalcopyrite, pyrite and S^0 showed increased isoelectric points (pH 3.4-3.7) compared to the ones grown on ferrous sulfate (~ pH 2.5). Also, they were more hydrophobic and expressed more surface proteins than ferrous sulfate grown cells (He et al. 2008).

The recent described candidatus *Acidianus copahuensis* showed growth flexibility and physiological versatility (Giaveno et al. 2013). Sulfur oxidation key enzymes like SOR present in *A. brierleyi* (Kletzin et al. 2004) were also detected to be encoded in a draft genome sequence of *A. copahuensis*. Also,

homologous genes of the Fox cluster enzymes, associated with iron oxidation, were found. The presence of *aioAB* genes encoding arsenite oxidase, suggest the ability to utilize arsenite as electron donor (Urbieta et al. 2014). These genes have been reported in *Acidianus hospitalis* and *Sulfolobus tokodaii* genomes, but not in other members of *Sulfolobales*.

1.4.3 The genus *Sulfolobus*

The first species of *Sulfolobus* (*Sulfolobus acidocaldarius*) was isolated from a hot spring at Yellowstone National Park. It is an aerobic and heterotrophic thermophile. Currently, there are 7 described species within the genus *Sulfolobus* (Table 1). Although exhibiting 99.8 % identical 16S rRNA sequences of the *Sulfolobus* species, a small but significant level of genetic differentiation among the populations from Yellowstone National Park, Lassen Volcanic Park (Iceland), Uzon Caldera (Russia), and Mutnovsky Volcano (Russia) has been detected (Whitaker et al. 2003).

S. metallicus is one of the most often used thermophiles for leaching of MS. It is a thermo-acidophilic obligate aerobe with an optimal growth temperature of 65 °C and a growth pH of 2-3. It was first isolated from a solfataric field in Krafla, Iceland (Huber and Stetter 1991), and it oxidizes iron(II) ions, reduced inorganic sulfur compounds (RISCs) (e.g. S^0, tetrathionate) and MS. *S. metallicus* is the only species of this genus, which can grow chemolithotrophically using MS or RISCs to sustain growth. Based on 16S rRNA sequences it is classified as a single phylogenetic clade inside the four groups of the genus *Sulfolobus* (Huber and Prangishvili 2006). In addition, compared to the mesophilic and moderately thermophilic archaeal and bacterial counterparts, *S. metallicus* grows at higher temperatures (~ 65 °C), leading to increased MS leaching rates.

Bioleaching of pyrite by *S. metallicus* was shown to be influenced by particle size and pulp density. The presence of fine particles (size fraction below 25 µm)

or high pulp density (above 18 %) apparently damaged the structure of the cells, resulting in their inability to oxidize pyrite (Nemati and Harrison 2000b; Nemati et al. 2000).

Bioleaching of chalcopyrite by *S. metallicus* is conducted in a cooperative action between attached cells which can oxidize sulfur-containing surface layers on chalcopyrite, forming thiosulfate, sulfite and bisulfite, and planktonic cells, which further oxidize these intermediate compounds to bisulfate and sulfate. Attached cells play important role in the removal of surface passivating layers. Thus, the oxidative action of iron(III) on chalcopyrite is greatly enhanced (Gautier et al. 2008). In addition, the efficient process of oxidation of residual sulfur compounds, i.e. sulfur and polysulfides, formed during the chemical dissolution of the MS, contributes to a significant increase in copper dissolution rates (Jordan et al. 2006).

1.5 Attachment, EPS and biofilm of acidophiles

Microorganisms are well known for their unique ability to thrive in different lifestyles (e.g. planktonic or sessile) and environments, even within extreme ones. The most common and widespread lifestyle of microbes on earth is in form of biofilms, which are associated colonies of microbes embedded in a matrix of EPS. Biofilms can be found as surface-associated or "floating mats", occurring in air-water interfaces. The biofilm lifestyle protects cells from environmental stress like desiccation, nutrient starvation, radiation and/or oxidative stress (Flemming and Wingender 2010). Biofilm lifestyle generally includes five stages: initial attachment, irreversible attachment, biofilm development, maturation, and dispersal (Fig. 3).

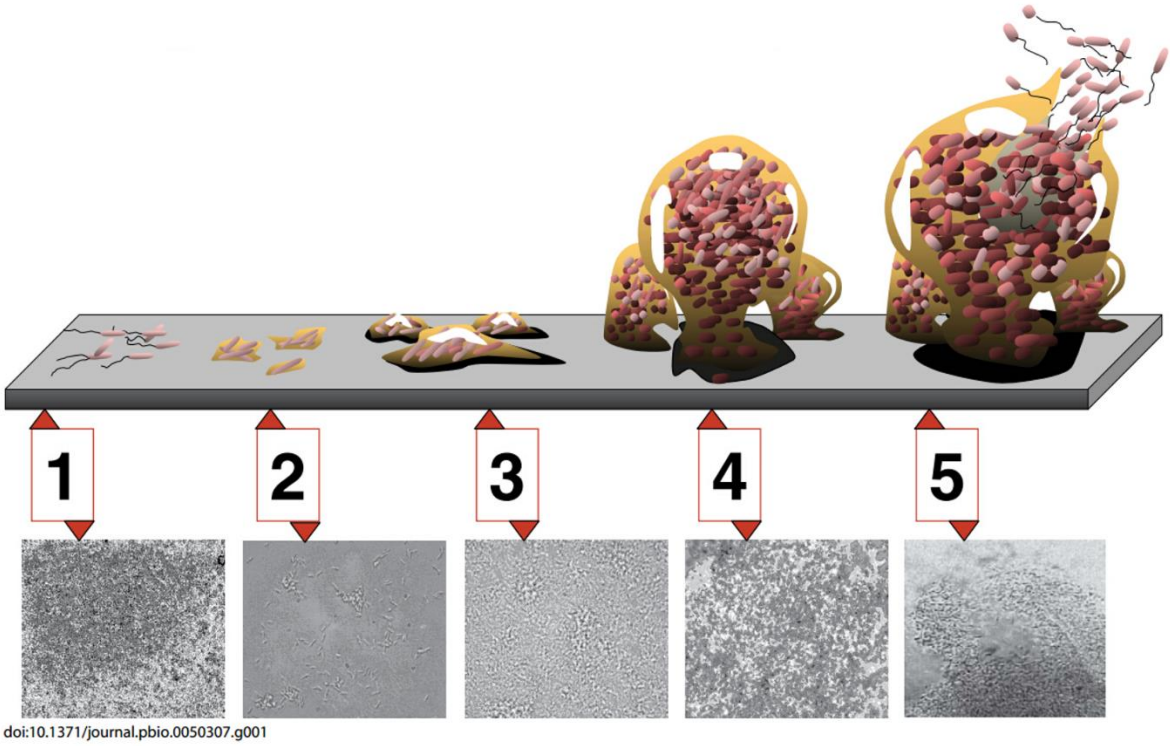

Figure 3. The five stages of biofilm lifestyle. The current model of biofilm development is a complex developmental process including five distinct stages. Stage 1, initial attachment; stage 2, irreversible attachment; stage 3, maturation I; stage 4, maturation II; stage 5, dispersion. Each stage of development in the diagram is paired with a photomicrograph of a developing *Pseudomonas aeruginosa* biofilm (Monroe 2007).

The EPS matrix is highly hydrated and up to 97 % of biofilm is composed of water (Zhang et al. 1998). It consists of different compounds like proteins, carbohydrates, extracellular DNA (eDNA), detritus or trace amount of metal ions. EPS enable the formation of 3-dimensional biofilm structures. They also play essential roles in mediating cellular attachment and cell-surface connections. The composition varies among different species and growth conditions (Gehrke et al. 1998; Flemming and Wingender 2010).

1.5.1 Attachment of acidophiles to surfaces

It has been shown that attachment of bioleaching microorganisms to MS surface does not occur randomly (Shrihari 1995; Dziurla et al. 1998; Edwards et al. 2001; Gehrke et al. 2001; Noël et al. 2010). Cells of *At. ferrooxidans* and other acidophiles preferentially attach to grain boundaries and sites with visible surface faults e.g. pores, cracks, etc. Cell attachment to pyrite surfaces with a low degree of crystallization seem to be favored, resulting in cell orientation along crystallographic axes, in whose direction oxidation fronts propagate (Sanhueza et al. 1999). *At. ferrooxidans* cells selectively attached to iron containing minerals pyrite or chalcopyrite but not quartz or galena (Ohmura et al. 1993; Harneit et al. 2006). Cell adhesion to pores and scratches may be due to contact area enhancement and protection from weak shear forces. In contrast, cell attachment to areas with low crystallization not often related to changes in surface topography. Therefore, the presence of some attractants may explain attachment to specific sites on the mineral surface. Several strains of *At. ferrooxidans* and *Leptospirillum ferrooxidans* have been shown to possess chemosensory systems (Acuna et al. 1992; Meyer 2002). Chemotaxis and attraction to gradients of iron(II)/(III) ions, thiosulfate and other compounds may occur compulsorily during MS dissolution. Recent work using atomic force microscopy (AFM) equipped with a Kelvin probe indicates that the cells of *L. ferrooxidans* attached to pyrite surfaces which are more negatively charged (about 100-200 mV) than the surrounding areas (Vera et al. 2013b). In a similar case, it was observed that sulfate-reducing bacteria (*Pseudomonas* sp.) attached in the immediate vicinity (nanometer range) of the anode on steel surfaces. The anode was negatively charged until a release of iron(II) ions occurred. As a consequence of bacterial attachment, the anode and the cathode became permanent (manifest), and steel dissolution commenced (Little et al. 2000).

At. ferrooxidans cells cultivated with chalcopyrite showed the strongest interaction forces with the same substrate. Those compared with the ones of

cells cultivated with iron(II) ions or S^0 were considerably lower. Also, chalcopyrite leaching efficiency and initial cell attachment rate were found to be correlated with cell adhesion forces (Zhu et al. 2015). Among the three species *At. ferrooxidans*, *Acidithiobacillus thiooxidans* and *L. ferrooxidans*, the latter one showed the highest adhesion force to chalcopyrite. EPS-deficient cells, obtained after EDTA extraction, exhibited reduced initial attachment rate and adhesion forces to chalcopyrite (Zhu et al. 2012).

It has been shown that in binary species biofilms the presence of active biofilms of iron-oxidizers may influence subsequent cell attachment by other species. *At. thiooxidans* cells attached 40 % more to pyrite precolonized with biofilms of *At. ferrooxidans* or *L. ferrooxidans*. Interestingly, its cell attachment was faster to pyrite precolonized with *L. ferrooxidans* than with *At. ferrooxidans*. As *L. ferrooxidans* leach pyrite more efficiently than *At. ferrooxidans*, the faster attachment observed for *At. thiooxidans* may be related to a chemotactic response towards RISCs like thiosulfate which are known to be released after pyrite leaching (Bellenberg et al. 2014). The analysis of the complete *At. thiooxidans* genome sequence revealed a complete suite of genes for flagellar formation and chemotaxis (Valdes et al. 2011). In contrast, the cell attachment of *At. ferrooxidans* to pyrite grains precolonized with *L. ferrooxidans* was strongly dependent on its pre-cultivation. Thiosulfate-grown cells were positively influenced by the presence of *L. ferrooxidans*, while iron(II)-grown cells were not (Bellenberg et al. 2014). Summarizing, the presence of iron oxidizers, which have been described as primary colonizers in natural AMD biofilms (Wilmes et al. 2009) may be a relevant factor for sulfur-oxidizers to efficiently attach to MS.

1.5.2 Biofilms of acidophiles

In general, acidophilic bacteria and archaea showed preferential attachment to defect sites present on S^0 surface. This has been observed for cells of *At.*

thiooxidans (Schaeffer et al. 1963), *Sulfolobus* sp. (Weiss 1973), *Thiobacillus denitrificans* (Baldensperger et al. 1974) and *At. ferrooxidans* (Espejo and Romero 1987). Cell wall components like a glycocalyx and cell appendages such as pili were found to be involved in connecting cells of *Sulfolobus* sp. and *Thiobacillus albertis* with S^0 (Weiss 1973; Bryant et al. 1983; Bryant et al. 1984; Laishley et al. 1986). Additionally, membrane blebs were visualized and these were hypothesized to aid the cells by overcoming the hydrophobic barrier necessary for their growth on S^0 (Knickerbocker et al. 2000; Crescenzi et al. 2006).

Biofilm formation and EPS production on MS have been studied for acidophilic bacteria and archaea. In general, cells are also forming monolayer biofilms and show selective attachment, preferentially to sites with crystal defects, fractures and pores. Examples of these observations include visualization of cells of *Caldariella* (a thermo-acidophilic archaeon) on pyrite or chalcopyrite (Murr and Berry 1976), *At. ferrooxidans* on pyrite or chalcopyrite (Wakao et al. 1984; Gehrke et al. 1998; Sanhueza et al. 1999; Sampson et al. 2000; Tributsch and Rojas-Chapana 2000; Lei et al. 2009; Noël et al. 2010; Bellenberg et al. 2015), *A. caldus* on pyrite (Edwards et al. 2000a) and enrichment cultures obtained from the Iron Mountain in California on pyrite surfaces (Edwards et al. 1998; Edwards et al. 1999). In contrast, an *in situ* AFM analysis of *Sulfobacillus thermosulfidooxidans* attached to pyrite indicated that cells on the surface were distributed in small clusters instead of forming a continuous biofilm. No evidence was found to suggest a preferential attachment to certain sites or a preferred orientation (Becker et al. 2011). Also, cell attachment of *Metallosphaera sedula* and *S. metallicus* show no preferential orientation. However, pyrite oxidation and pit etching were influenced by surface symmetries (Etzel et al. 2008). Interestingly, two distinct biofilm morphologies were described for an extremely acidophilic archaeon *F. acidarmanus* Fer1. A multilayer biofilm was developed on pyrite surfaces, and up to 5 mm-long

filaments were found on sintered glass spargers taken from gas lift bioreactors (Baker-Austin et al. 2010). Cells of *M. sedula* were found to be wiggling along the metal ore by epifluorescence microscopy (EFM), suggesting that cell appendages were involved in cell attachment to the ore (Huber et al. 1989). Interactions of three axenic cultures of thermophiles *A. brierleyi*, *M. sedula* and *S. metallicus* with pyrite were first documented using SEM and TEM. Several of deposited structures were formed on the pyrite surface, including sub-micron precipitates and disc-shaped structures (Mikkelsen et al. 2007).

The molecular mechanisms controlling biofilm formation in acidophilic metal/sulfur-oxidizing archaea are far less explored (Orell et al. 2013). Preliminary work on crenarchaeal biofilms on other surfaces with respect to their morphology, architecture and chemical components has been done. The first crenarchaeal biofilm analysis was described for three closely related *Sulfolobus* sp. Biofilms with "carpet-like" structures by *S. solfataricus* and *S. tokodaii* and high-density "tower-like" structures by *S. acidocaldarius* were observed (Koerdt et al. 2010). Cell appendages such as pili or flagella were proven to be involved in initial attachment of *S. solfataricus* to various surfaces, including glass, mica, pyrite and carbon-coated gold grids (Zolghadr et al. 2010). Also, three type IV pili-like cell appendages of *S. acidocaldarius* were found to be differently involved in cell colonization and biofilm formation on glass (Henche et al. 2012). The enzyme mannosidase in *S. solfataricus* was found to be important in archaeal biofilm formation and modulation of EPS composition (Koerdt et al. 2012).

Biofilm detachment as well as cell dispersal of acidophilic biofilms is still largely unknown. However, there are observations that acidophiles show such a behavior since footprints have been detected. Microbial footprints are composed mainly of EPS which are left on surfaces due to cell detachment or mechanical removal (Neu and Marshall 1990; Neu and Marshall 1991). Footprints have been described for *Thiobacillus intermedius* on iron (Telegdi et al. 1998), *At.*

ferrooxidans (Rojas-Chapana et al. 1996; Mangold et al. 2008), *Sb. thermosulfidooxidans* (Becker et al. 2011) and a mixed culture of mesoacidophilic chemolithotrophs (Ghorbani et al. 2012). It has been reported that EPS compounds like lipopolysaccharides might detach from biofilms during their maturation (Jiao et al. 2010). Recent work in our laboratory has demonstrated different dynamics of colonization, biofilm formation and cell detachment of iron-oxidizing *Acidithiobacillus* and *Leptospirillum*. In this case the biofilms formed by the latter species are stable for longer incubation periods than the ones formed by iron-oxidizing acidithiobacilli (Bellenberg & Vera, unpublished results). Probably these detachment processes form part of a response to oxidative stress caused by the presence of reactive oxygen species (ROS) (Bellenberg et al. 2015), the increase of the ionic strength and the decrease of the pH.

1.5.3 Extracellular polymeric substances of acidophiles

In case of biofilm forming cells the dissolution process occurs within the EPS layer (Fig. 4), which can be considered a reaction space filling the volume between the outer cell membrane and the surface of the MS. Tributsch and co-workers demonstrated that this distance is 10-100 nm wide (Rodriguez-Leiva and Tributsch 1988). The thickness of *At. ferrooxidans* EPS was estimated for iron(II)-grown cells by *in vivo* AFM to be 28.7 nm (±13.5) (Taylor and Lower 2008). The EPS thickness of S^0- or pyrite-grown cells *in vivo* has not been reported yet. These values probably are higher than the above mentioned ones due to the fact that EPS levels are enhanced when the bacteria are grown with solid substrates (Sand et al. 1998).

The first comprehensive EPS analysis of leaching microorganisms was done for *At. ferrooxidans* strain R1. Pyrite-grown cells had a similar EPS composition compared to iron(II)-grown cells. These EPS consist of the monosaccharides glucose, rhamnose, fucose, xylose, mannose, C12-C20 saturated fatty acids,

glucuronic acid, and iron(III) ions (Gehrke et al. 1998; Gehrke et al. 2001). However, pyrite-grown cells possessed more than ten-fold amount of EPS. The initial attachment is mainly driven by electrostatic interactions (in which most likely 2 moles negatively charged glucuronic acid residues complex 1 mole positively charged iron(III) ions resulting in a net positive charge) with the negatively charged pyrite surface (at pH 2) in sulfuric acid solution (Solari et al. 1992; Blake et al. 1994).

Cells grown on S^0 do not attach well to pyrite, since their EPS composition is different compared to pyrite-grown ones. Their EPS contain considerably less monosaccharides and lack uronic acids, resulting in a complete absence of complexed iron(III) ions or other positively charged ions. However, EPS from S^0-grown cells do possess much more fatty acids than EPS from pyrite-grown cells. Consequently, it seems that hydrophobic interactions are exclusively relevant for attachment of cells of *At. ferrooxidans* to S^0 (Gehrke et al. 1998). Cell surface charge of *At. ferrooxidans* is different from soluble iron(II)-grown cells compared to solid substrate grown ones. Cells possess a higher amount of protein when grown on insoluble substrates such as pyrite or S^0 compared to cells grown with iron(II) ions (Sharma et al. 2003). The formation of capsular polysaccharides (CPS) of *At. ferrooxidans*^{T} occurred within the first 24 h of contact with pyrite (Bellenberg et al. 2012).

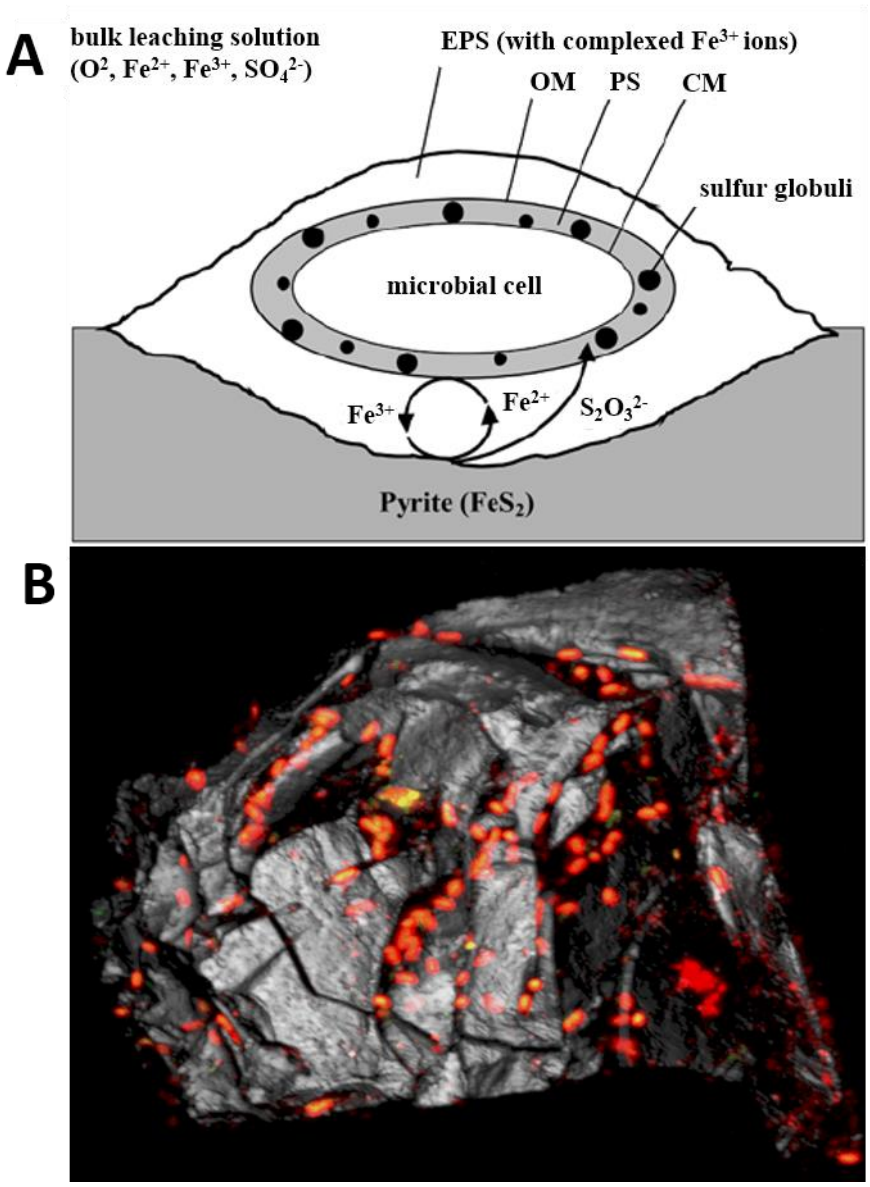

Figure 4. Model for contact leaching catalyzed by a microbial cell (modified from Vera et al. 2013b). A: Overview showing a biofilm cell embedded in the EPS layer attached to pyrite. Compounds like Iron(II)/(III) ions, thiosulfate present during MS dissolution are shown. CM, cytoplasmic membrane; PS, periplasmic space; OM, outer membrane. B: CLSM image showing a 3-D projection of a pyrite grain (50-100 µm) colonized with cells of *At. ferrooxidans*^{T}. Cells were stained with Syto 9 (green) for nucleic acids and lectin Con A. Color allocation: green=Syto 9, red=/Con A-tetramethyl rhodamine isothiocyanate (TRITC), grey=reflection. The merged image from all three channels is shown.

There are several methods for extraction of EPS, these comprise physical and chemical ones. Isolation of EPS from *Acidiphilum* 3.2Sup(5) was comparatively

done by using five methods: EDTA, NaOH, ion exchange resin, heating and centrifugation. The extracted EPS mainly contained carbohydrates and proteins regardless of the extraction method. However, higher EPS amounts as well as a less degree of cell lysis were achieved by using EDTA than by the other methods. This study confirmed that both, the amount and the chemical composition of EPS, strongly depend on the applied extraction method (Tapia et al. 2009).

EPS production in stirred reactors processing cobaltiferous pyrite concentrate was studied in order to optimize bioleaching processes. Bacterial attachment and leaching efficiency were both decreased in accordance with reduced levels of EPS production under N limitation. CO_2 limitation caused a significant decrease of exopolysaccharide production (d'Hugues et al. 2008). Analyses of the EPS extracted from several continuously operated bioleaching systems indicated that the EPS consisted mainly of carbohydrates, smaller amount proteins and uronic acids (Govender and Gericke 2011). Characterization of two acidophilic microbial biofilms from Iron Mountain, California showed that their EPS were composed of carbohydrates, metals, proteins and minor quantities of DNA and lipids (Jiao et al. 2010).

Recently, several chemical mapping techniques have been used to *in situ* analyze EPS components of acidophiles. Synchrotron radiation based scanning transmission X-ray microscopy (STXM) imaging and micro X-ray fluorescence (μ-XRF) mapping have been used to study extracellular thiol groups (-SH) of *At. ferrooxidans* cells. It was shown that the -SH content of *At. ferrooxidans* grown on S^0 was four times higher than those contents of iron(II)-grown cells. These data suggest that extracellular -SH groups may play an important role in sulfur activation prior to its oxidation (Xia et al. 2013). STXM has been also used to visually analyze EPS of *At. ferrooxidans* on pyrite. The distribution of polysaccharides and proteins in biofilms was visually correlated with the optical overview. In addition, polysaccharide-rich compounds were often detected at

the pyrite-cell boundaries, while lipid- and protein-rich ones were found in the cell center regions (Mitsunobu et al. 2015).

1.6 Analytical techniques for biofilm and EPS study

1.6.1 Atomic force microscopy

AFM belongs to the group of scanning-probe microscopies (SPMs) which is based on the interactions of electron tunnelling current of a metal tip with surfaces (Binnig et al. 1982). The appearance of AFM was in the mid-1980s (Binnig et al. 1986). During the past of decades, improvement of instrumentation, sample preparation and testing conditions has enabled AFM a powerful tool to explore biological structures like cell surfaces and biological molecules (Dufrêne 2004).

The key feature of an AFM is the cantilever (Fig. 5). AFM operates by sensing the small forces acting between the sample surface and a sharp tip which is fixed on a cantilever. The interaction forces with the sample cause the cantilever to bend and deflect. The deflection of cantilever is detected by a laser beam reflected from the free end of the cantilever into a photodiode. The topographic information collected by photodiode is shown in the imaging mode in computer system with special software (e.g. JPK, Berlin) and a 3D image of the surface architecture with (near) molecular resolution is available. AFM cantilevers and tips are usually made of silicon or silicon nitride using microfabrication techniques. Also, newly developed probes are chemically functionalized, coated with bacteria or biomacromolecules for studying cell-surface interactions (Dorobantu et al. 2012). These AFM probes coated with acidophilic bacteria allow to measure interactive forces between bioleaching microorganisms and mineral surfaces (Zhu et al. 2012; Diao et al. 2014a; Diao et al. 2014b). By combination with other techniques, e.g. a Kelvin probe, relative surface potential differences and charge distributions on the surface can be measured (Vera et al. 2013b).

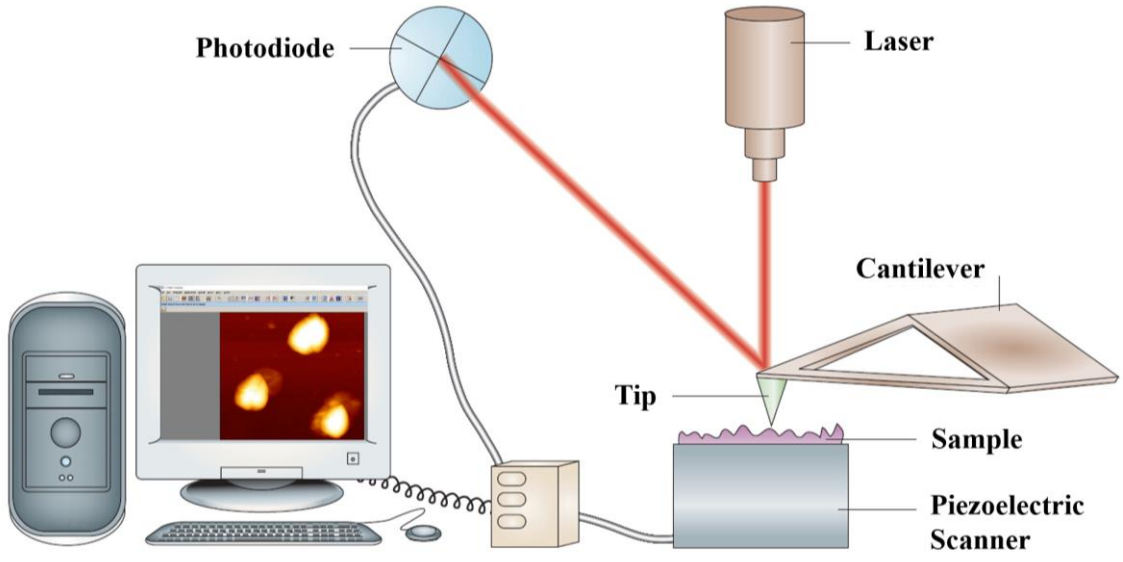

Figure 5. Schematic of AFM working principles (modified from Dufrêne 2004).

The concept of SPMs is the generation of images of surfaces by measuring the physical interaction between a sharp tip and the sample rather than by using an incident beam (light or electrons) as in classical microscopy. The main parts of an atomic force microscope are the sample stage, the cantilever and the optical detection system, which comprises a laser diode and a photodetector. The sample is moved relative to the cantilever in three dimensions using piezoelectric ceramics. The force interacting between the tip and the sample is monitored with pico-newton (10-12 N) sensitivity, by attaching the tip to a soft cantilever, which acts as a spring, and measuring the bending (or deflection) of the cantilever. The cantilever deflection is usually detected by a laser beam focused on the free end of the cantilever and is reflected into a photodiode.

1.6.2 Confocal laser scanning microscopy and Epifluorescence microscopy

CLSM in combination with fluorescent probes provide detailed 3-dimensional structure and compositional information (Lawrence et al. 2003; Neu and Lawrence 2014a). The main advantage of CLSM is its 3-dimensional sectioning capability of fully hydrated, living microbial communities. It allows multi-channel (up to 5) imaging of cellular and EPS constituents in the biofilm matrix. The digital image series or stacks recorded can be used for visualization and

quantification (Neu and Lawrence 2014b). The advantages of CLSM are flexible sample mounting (upright/inverted); high-resolution; optical sectioning; multichannel imaging; sequential/simultaneous; ideal for motile objects and fast processes; options for other light sources; imaging in deep locations; possibility to use excitation of UV fluorochromes and organic substances (Neu and Lawrence 2015).

In CLSM a biological sample is sectioned optically resulting in crisp images without a blurred signal from other optical planes. Single sections, or in most cases series of sections, are recorded as 2-dimensional images that finally will allow 3-dimensional reconstruction with the help of various imaging softwares like IMARIS (Bitplane AG, Zurich) or ImageJ (Abramoff et al. 2004). For this purpose the sample has to be stained with fluorochromes that are specific for certain compounds e.g. glycoconjugates or proteins. In addition, the autofluorescence and the reflection signals may be recorded. This enables to simultaneously visualize different biofilm compounds *in situ*.

A major characteristic of a CLSM set-up is the laser lines available for excitation of fluorochromes. The laser options for excitation include traditional gas lasers (e.g. Ar, He/Ne), laser diodes, two-photon lasers and super-continuum white light sources (Neu and Lawrence 2015). The possible wavelengths range from UV to IR (infra-red). Three laser lines at 488, 561, and 633 nm are usually available. These three lines are sufficient for most samples and cover many of the popular fluorochromes.

The potential of CLSM for complex biofilm visualization was first demonstrated by investigation of *Pseudomonas fluorescens* biofilms. This study showed that quantitative visualizations of 2D (both xy and xz), 3D, and potentially 4D (time course) reconstructions of pure and mixed-species biofilm characteristics were possible (Lawrence et al. 1991). Since then, large amount of publications on biofilm studies are available by using CLSM techniques (Neu and Lawrence 2014b).

EFM is a fast and convenient tool for visualization of complex biological samples like biofilms by fluorescence labelling of DNA, carbohydrates, proteins or lipids. However, like other light microscopes, the resolving power of EFM is limited by diffraction to half the wavelengths of the light used. Therefore, the combination of AFM & EFM takes both advantages that AFM has excellent spatial resolution, whereas EFM offers excellent biological identification properties. The combination of two microscopic techniques can be readily realized by applying a shuttle stage. This shuttle stage carries the actual sample precisely fixed on a glass slide. It could be transferred between the atomic force microscope and the epifluorescence microscope, resulting an exact positioning of the stage on both microscopes. Error of the sample location is no more than 3 to 5 µm (Mangold et al. 2008). The combination of AFM and EFM allows for confirmation of biological or chemical origins of structures at a high resolution (Mangold et al. 2008). Surface properties of minerals and their modification due to microbial activities can be recorded. In addition, the probes used (e.g. fluorescently labeled lectins) can provide additional biochemical information of the biofilm cells. The formation of monolayer biofilms as well as EPS production were found for cells of *Metallosphaera hakonensis* on chalcopyrite (Africa et al. 2013), *At. ferrooxidans* and mixed cultures of *At. thiooxidans* and *At. ferrooxidans* on pyrite (Harneit et al. 2006; Florian et al. 2010; Noël et al. 2010; Florian et al. 2011; Gonzalez et al. 2013). The biofilm formation was accompanied with the production of EPS containing mannose or glucose.

1.6.3 Fluorescence lectin-binding analysis

EPS represent a crucial part of microbial biofilms and a key element in terms of biofilm functionality (Neu and Lawrence 2009). Due to the complexity of EPS, an *in situ* approach to analyze the EPS glycoconjugates by means of fluorescence lectin binding analysis (FLBA) has been developed (Staudt et al. 2003; Peltola et al. 2008; Zippel and Neu 2011; Bennke et al. 2013; Castro et al.

2014). FLBA allows simultaneous visualization and characterization of EPS glycoconjugates based on the lectin specificities. A requirement for FLBA is that lectins shall be tested against a specific biofilm sample (Neu et al. 2001). It is necessary due to the fact that a specific biofilm is stainable only by certain lectins. Normally, this screening allows to select suitable lectins for a particular biofilm sample. Additional EPS components can be visually characterized by combination with other stains specific for proteins, nucleic acids or lipids, among others (Neu and Lawrence 2014a; Neu and Lawrence 2014b). For instance, the Syto and Sypro series are used to detect cells via their nucleic acids and cellular proteins, respectively. FM dyes (FM1-43 and FM4-64) and Nile red are specific to stain membranes and lipophilic compounds. These stains can be used also to stain extracellular compounds in biofilms (Lawrence et al. 2007; Neu and Lawrence 2014a). DDAO (7-hydroxy-9H-1,3-dichloro-9,9-dimethylacridine-2-one) stains nucleic acids and normally does not penetrate cell membranes. Thus, it has been selected as the preferred fluorochrome for staining eDNA (Koerdt et al. 2010). Combination of several types of stains allowed us to get detailed information about biofilms of acidophiles on different energetic substrates.

Lectins are a group of proteins or glycoproteins, which are capable of binding reversibly and specifically to carbohydrates without altering their structures. They are originally called ñhemagglutininsò, or more precisely ñphytohemagglutininsò due to their ability to agglutinate erythrocytes (Sharon and Lis 1972; Lis and Sharon 1973). It is generally believed that Peter Hermann Stillmark first described a lectin in his doctoral thesis presented in 1888 to the University of Dorpat (now Tartu, Estonia). This hemagglutinin named ricin was highly toxic and isolated from seeds of the castor tree (*Ricinus communis*). The sugar specificity of lectins was first demonstrated by sugar inhibition tests. It was found that hemagglutination by Concanavalin A was inhibited by sucrose (Sumner and Howell 1936).

At present, more than 70 lectins are commercially available. These mainly include plant lectins and few other lectins like bacterial lectins, algal lectins, animal lectins, fungal lectins, and virus lectins. More than 200 lectin primary and 3D structures are available in the "Lectin" database (http://glyco3d.cermav.cnrs.fr/search.php?type=lectin).

1.6.4 Fourier transform infrared spectroscopy

Fourier transform infrared (FTIR) spectroscopy is a technique used to obtain an infrared spectrum of absorption, emission, photoconductivity or Raman scattering of a solid, liquid or gas materials. Basically, FTIR spectrum radiation is simultaneously recorded by an interferometric system like Michelson interferometer. The signal measured at the detector which is called interferogram contains all the information of the sample over all wavelengths. The sample-spectrum is then calculated from the interferogram by fast Fourier transform (FT) techniques with elaborated mathematical algorithms.

FTIR spectroscopy offers molecular-scale information on both organic and inorganic constituents for surface characterization. It is widely used to analyze functional groups in environmental samples and also to identify microbes at the strain level according to their specific surface infra-red spectra (Naumann et al. 1991; Schmitt and Flemming 1998; Santos et al. 2010; Alvarez-Ordonez et al. 2011; Liu et al. 2015). In addition, main absorption peak ratios within a defined spectrum of a biological sample can correlate with the composition of biological materials and provide useful information on the composition of environmental biofilm samples (Nichols et al. 1985; Sheng et al. 2006).

For attenuated total reflectance (ATR)-FTIR spectroscopy, IR radiation is multiply reflected on an inner surface (Germanium or diamond) of an internal reflection element (IRE). The radiation penetrates from the IRE into the adjacent environment exponentially decays to zero within approximately 1 µm of the IRE's surface. This radiation termed an evanescent wave can be absorbed

by compounds near the surface, thus producing IR absorption bands. ATR-FTIR spectroscopy has been applied to observe biofilm forming directly on the interface of an ATR crystal. A spectrum is acquired non-destructively, *in situ* and in real time. This method is suitable for fundamental biofilm research, as well as for monitoring of bacterial adhesion and biofilm formation process (Watkinson et al. 1994; Parikh and Chorover 2006; Quilès et al. 2010).

2. Aims of the Study

To date, EPS production and biofilms of archaeal species have been investigated only to a limited extent, especially meso and thermoacidophilic ones. In addition, it is essential to visualize EPS glycoconjugates with regards to i) their identity and ii) their distribution on relevant surfaces. The analysis of EPS chemical composition may contribute to understand their function(s) in bioleaching.

The present work was focused on biofilms of acidophilic archaea with surfaces such as MS (i.e. pyrite or S^0) during bioleaching. Three representative species of iron and/or sulfur-oxidizing archaea, the mesophile *F. acidiphilum* DSM 28986 (former BRGM4), and the thermophiles *S. metallicus* DSM 6482^T and *Acidianus* sp. DSM 29099 (former RZ1), were used.

The study aimed to investigate:

(1) How is their initial attachment behavior to MS such as pyrite or chalcopyrite or S^0?

(2) What are the surface/extracellular compounds involved in the initial attachment?

(3) What are the main features of the archaeal biofilms developed on these surfaces?

(4) Which lectins bind each strain and is it feasible to use a lectin-based approach to distinguish dual-species biofilms?

(5) The composition of the EPS of these strains and how it is influenced by growth conditions e.g. different substrates such as iron(II) ions, pyrite or S^0?

3. Materials and Methods

3.1 Strains and cultivation

F. acidiphilum DSM 28986 (former BRGM4), isolated from a stirred tank reactor (Bryan et al. 2009), was kindly provided by Prof. D. B. Johnson at University of Bangor, UK. *S. metallicus* DSM 6482^{T} was purchased from Deutsche Sammlung von Mikroorganismen und Zellkulturen GmbH (DSMZ; Braunschweig, Germany). Strain *Acidianus* sp. DSM 29099, an iron- and sulfur-oxidizer, was isolated from a hot spring at Copahue Volcano, Neuquén, Argentina in the autumn of 2011. All strains were cultivated in Mackintosh basal salt medium (MAC) (Mackintosh 1978) containing 0.02 % yeast extract with an initial pH 1.7 for *F. acidiphilum* DSM 28986 or pH 2.5 for *S. metallicus*^{T} and *Acidianus* sp. DSM 29099, respectively. *F. acidiphilum* DSM 28986 was grown at 37 ¯C with 4 g/L iron(II) ions. *S. metallicus*^{T} and *Acidianus* sp. DSM 29099 were grown at 65 ¯C with 10 g/L S^{0}. Cells were cultivated aerobically either in Erlenmeyer flasks under shaking at around 120 rpm or in 5 L bottles with aeration (sterile air; ~15 L/h) and agitation at 180 rpm by placing a magnet bar in the bottle bottom.

3.2 Substratum, biofilm formation and pyrite leaching

Pyrite slices with a size of approx. 1 cm × 1 cm × 2 mm were cut from cubes (origin Navajun, Spain) by using a diamond cut-off wheel (B 127, Ø 127, thickness 0.48, arbor size 12.7 mm) in the laboratory of the Department of Material Science and Engineering. Grains were prepared by crushing and grounding pyrite crystals using a jaw-crusher (BB 1/A, Retsch, Germany) and a disc-swing-mill (HSM 100M, Herzog, 1988) in the laboratory of the Department of Geology. Pyrite grains with a size of 50-100 µm and 200-500 µm were selected by wet sieving using Retsch sieves (Retsch, Germany). Both, slices and grains, were washed with boiling 6 M HCl for 30 min, rinsed twice

with deionized water, and three times with acetone as described previously (Schippers et al. 1996). After cleaning, pyrite was dried at 80 °C sterilized for 24 h at 120 °C under a

To produce S^0 prills and cubes, S^0 powder (Carl Roth, Germany) was molten in a glass beaker at 130 °C and poured into cold deionized water with vigorous agitation (250 rpm). S^0 prills with a diameter of 1-3 mm were formed due to rapid cooling. Also, molten S^0 was poured on glass plates to obtain a S^0 layer after its solidification. S^0 coupons with a size of approx. 0.5 cm × 0.5 cm × 2 mm were obtained by manually breaking the S^0 layer. Both, S^0 prills and coupons, were autoclaved at 110 °C fo

For attachment assays, cells were harvested at 8000 rpm (11300 g) for 15 minutes at 20 °C. Cell pellets were washed and resuspended in washing solution (MAC medium supplemented with 0.2 g/L iron(III) ions). This cell suspension was kept at 17 °C for 24 h to replenish EPS. Initial cell number 2-3×10^8 cells/mL was inoculated with 10 g pyrite or S^0 in 50 mL MAC medium. Cell number was monitored for 6 h. The attached cell number was determined by subtracting the planktonic from the initial cell number. Triplicates were done for the attachment tests.

To allow biofilm formation, 20 g pyrite grains (200-500 µm) or S^0 prills were incubated with pure cultures of test organisms in 300 mL MAC medium (initial cell concentration ~1×10^8 cells/mL). In case of pyrite or S^0 coupons, 5-10 slices were placed in a 100-mL wide-neck Erlenmeyer flask containing 50 mL MAC medium. Both pyrite and S^0 substrates colonized with cells were withdrawn for staining and microscopic observations (see subchapters 3.5, 3.6 and 3.7).

For bioleaching tests, 300-mL Erlenmeyer flasks containing 5 g of pyrite grains (50-100 µm), 100 mL MAC medium (pH 1.7) and 0.2 g/L yeast extract were inoculated with pure cultures of test organisms at an initial cell number of ~1×10^8 cells/mL. Abiotic controls were also done. To determine leaching efficiency, iron ions were quantified as described in subchapter 3.3.

3.3 Cell number, pH and iron determination

The cell number in planktonic phase was determined using a Thoma counting chamber (depth = 0.1 mm, area per small square = 0.0025 m^2, Assistant, Germany) and a light microscope (Leica DMLS, Wetzlar GmbH) in phase contrast mode with 400× magnification.

The pH of samples was measured with a digital pH meter (Model pH 537, WTW, in Lab® 422 Combination Semi-micro pH Electrode, Mettler Toledo).

Iron determination was performed according to a ñ P h e n a n t h r o l i n e ò method (Tamura et al. 1974). Briefly, iron(II) ions and 1,10-Phenanthroline build a red colour complex, which can be determined spectrophotometrically at 492 nm. Upon addition of hydroxylamine iron(III) ions are reduced to iron(II) ions, whereby the total iron concentration was determined. Samples were measured in triplicate using a UV-VIS spectrophotometer (Cary 50, Varian INC.) equipped with software ADL Shell.

3.4 EPS extraction and chemical analysis

Planktonic cells in late exponential growth phase were separated from pyrite or sulfur prills by filtration through sterile Whatman filter paper. Cells were collected afterwards by centrifugation at 8000 rpm for 15 min. Cell pellets were washed by sterile MAC medium and freeze-dried (ALPHA 2-4 LSC, -80 °C). The supernatant was further filtrated through polycarbonate filters (GTTB, Ø2.5 cm, 0.2 µm pore size, Millipore®) to remove whole cells. These cell-free s u p e r n a t a n t s (c o n t a i n i n g ñ c o l l o i d a l membrane (cutoff 3.5 KDa) against deionized water at 4 °C for 48 h. Dialyzed colloidal EPS solutions were further freeze-dried. Capsular EPS were extracted from cell pellets using 20 mM EDTA as described previously (Castro et al. 2014). Sulfur particles were manually milled in a mortar and incubated with 20 mM EDTA at 4 °C and shaking at 180 rpm for 4 h to extract EPS from biofilm cells. Pyrite grains were directly incubated with 20 mM EDTA to extract EPS

from biofilm cells. The extraction was repeated three times and the resulting solutions were centrifuged, filtered and dialyzed as described above.

Phenol–sulfuric acid method was used for carbohydrate determination with glucose as a standard (Dubois et al. 1956). Protein concentration was analyzed with bovine serum albumin (BSA) standard (Bradford 1976). DNA was determined using DNA from salmon sperm as a standard (Burton 1956). Cell lysis was estimated by measuring glucose-6-phosphate dehydrogenase (G6PDH) activity (Ng and Dawes 1973).

3.5 Staining

The cell biomass and spatial distribution within the biofilms on pyrite or S^0 were visualized after staining with the nucleic acid stains: DAPI (diamidino-2-phenylindole), Syto 9, Syto 61, Syto 64, SybrGreen (Invitrogen, Germany) and DDAO (7-hydroxy-9H-1,3-dichloro-9,9-dimethylacridin-2-one; Invitrogen, Germany). The detailed information of these stains are shown in subchapters 4.2 and 4.3. The cell-permeant Syto 64, a fluorescent nucleic acid stain, exhibits bright red fluorescence upon binding to nucleic acids. Pyrite or S^0 samples with attached cells were washed three times with filter-sterilized tap water. Neutralized samples were mounted in a Petri dish or in a CoverWell chamber of 20 mm in diameter with 0.5 mm spacer (Invitrogen, Germany). DDAO was incubated with samples for 20 min before CLSM observation. All other dyes were added to the washed samples and directly visualized. Direct light exposure was avoided. Stains specific for proteins, polysaccharides were also tested to characterize biofilm components.

3.6 Fluorescence lectin-binding assays

Pyrite or S^0 samples were neutralized with filter-sterilized tap water and incubated with 0.1 mg/mL lectins for 20 min at room temperature in the dark. Lectin staining was done in a Petri dish or in a CoverWell chamber of 20 mm in

diameter with 0.5 mm spacer (Invitrogen, Germany). Afterwards, stained samples were washed three times with filter-sterilized tap water in order to remove unbound lectins. More than three pyrite grains or S^0 prills were checked by eye under microscope to make a decision whether a lectin bound or not bound to biofilm cells. In case of counter staining, lectin stained samples were incubated with nucleic acid/protein/lipid stains and directly observed using CLSM without any further treatment.

For staining cells from the planktonic phase, 1 mL of cultures grown for 4 days were filtered on polycarbonate filters (GTTB, Ø2.5 cm, 0.2 µm pore size, Millipore®) as described previously (Bellenberg et al. 2012) and incubated with fluorescent lectins for 20 min. After staining, cells were washed three times with filter-sterilized tap water. Filters with stained cells were then mounted using an anti-fading agent (Citifluor, Ltd. AF2) and covered by a coverslip prior to CLSM observation.

3.7 Confocal laser scanning microscopy

Examination of stained samples was performed using a TCS SP5X AOBS (Leica, Heidelberg, Germany), controlled by the LASAF 2.4.1 build 6384. The system was equipped with an upright microscope and a super continuum light source (470-670 nm) as well as a 405 nm pulsed laser diode. Images were collected with a 63× water immersion lens with a numerical aperture (NA) of 1.2 and a 63× water immersible lens with a NA of 0.9. Details of fluorescent dyes along with excitation and emission filters used are shown in subchapter 4.2. CLSM data sets were recorded in sequential mode to avoid cross talk of the fluorochromes between two different channels. Surface topography and texture of the pyrite as well as of the S^0 surface were recorded by using the CLSM in reflection mode.

3.8 Atomic force microscopy and Epifluorescence microscopy

The BioMaterial Workstation (JPK Instruments, Germany), a combination of a NanoWizard II atomic force microscope (JPK Instruments, Germany) with an upright epifluorescence microscope (AxioImager A1m, Zeiss, Germany), was used to visualize cell and EPS distribution on surfaces. For AFM imaging, a silicon cantilever CSC37-A (Mikromasch, Estonia) with the following features was used: typical length, 250 µm; width, 35 µm; thickness, 2 µm; resonance frequency, 41 kHz; and nominal force/spring constant, 0.65 N/m. Each AFM image consists of 512 by 512 or 1024 by 1024 pixels. AFM imaging was performed in contact mode in air. For visualization of morphology of planktonic cells, 20 µL of cell suspension were fixed spread by evaporation. For visualization of biofilm cells and EPS on pyrite slices or S^0 coupons, samples were washed three times with filter-sterilized tap water prior to staining. Cells and their EPS were stained by Syto 9 and TRITC labeled Con A, respectively as mentioned above. By using a shuttle stage, the same surface area of samples was both visualized by EFM and AFM with an error below 2 µm (Mangold et al. 2008). At least three different spots (around 100 by 100 µm) from each sample were checked and recorded by combined AFM and EFM.

3.9 Fourier transform infrared spectroscopy

Powdered cell pellets, colloidal EPS, and EPS extracted planktonic or biofilm cells were spread on a diamond attenuated total reflectance (ATR) apparatus (Pike Technologies, USA), separately attached to the FTIR. The spectra were recorded using an FTIR 430 spectrometer (JASCO, Japan). The baseline shift of blank spectra was corrected using Spectra Manager (JASCO, Japan). At least 64 scans, with a resolution of 4 cm^{-1}, were collected for all samples using the Happ-Genzel apodization function. Two measurements were done for each sample. As all cellular components possess characteristic absorbance

frequencies and primary molecular vibrations between 4000-550 wave numbers (Naumann et al. 1991), the FTIR scan was carried out in this region.

3.10 Digital image analysis

Fluorescence images were analyzed using an extended version of software ImageJ (http://imagej.nih.gov/ij/).

Maximum intensity (MIP), isosurface and XYZ projections of 3-dimensional data sets were produced with the software IMARIS version 7.3.1 (Bitplane AG, Zurich, Switzerland). In some cases, deconvolution of 3-dimensional data sets was processed to enhance the clarity of the images using Huygens ver. 14.06 (SVI, The Netherlands).

4. Results and Discussion

This part is divided into three sections according to the single publications generated within this thesis. At the beginning of each subchapter, a short interpretation of the section is given.

4.1 Biofilm formation by the extremely acidophilic archaeon *F. acidiphilum*

The genus *Ferroplasma* receives great interest with respect to their special physicological properties, e.g. extremely acidophilic and cell wall-lacking. Microbial attachment to solid substrates of acidophiles and cell surface propterties are of great importance for manipulation of bioleaching both in nature and in anthropogenic processes. In this work, we applied floating filter cultivation technique and microscopical techniques e.g. CLSM, AFM & EFM and SEM to investigate the biofilm development of *F. acidiphilum*. CLSM studies showed that biofilms were heterogeneously distributed on floating filters over time, and varied within the different growth conditions such as supplementation with glucose. Cells formed a monolayer biofilm on pyrite and were preferably attached to its surface imperfections such as cracks/defects. Biofilm and planktonic cells exhibited significant morphological differences as visualized by AFM.

Hydrometallurgy 150 (2014) 245–252

Contents lists available at ScienceDirect

Hydrometallurgy

journal homepage: www.elsevier.com/locate/hydromet

Colonization and biofilm formation of the extremely acidophilic archaeon *Ferroplasma acidiphilum*

Ruiyong Zhang [a], Sören Bellenberg [a], Laura Castro [b], Thomas R. Neu [c], Wolfgang Sand [a], Mario Vera [a,*]

[a] Aquatische Biotechnologie, Biofilm Centre, Universität Duisburg-Essen, 45141 Essen, Germany
[b] Department of Material Science and Metallurgical Engineering, Complutense University of Madrid, Av. Complutense s/n, 28040 Madrid, Spain
[c] Department of River Ecology, Helmholtz Centre for Environmental Research-UFZ, 39114 Magdeburg, Germany

ARTICLE INFO

Available online 10 July 2014

Keywords:
Bioleaching
Archaea
Biofilm
Fluorescence microscopy
Atomic force microscopy

ABSTRACT

Ferroplasma spp. are widely distributed in acid mine drainage (AMD) and biomining environments at mesophilic and moderately elevated temperatures, at low pH and high concentrations of iron and other metal ions. Microbial attachment and biofilm formation on metal sulfides are of great importance during bioleaching. In this work, several cultivation and microscopical techniques were applied to investigate the biofilm development of *Ferroplasma acidiphilum*. Biofilms were heterogeneously distributed on filters over time, and varied within the different growth conditions such as supplementation with glucose. Additionally, cell distribution, biofilm formation as well as EPS production of *F. acidiphilum* cells forming biofilms on pyrite were observed by confocal laser scanning microscopy (CLSM), scanning electron microscopy (SEM) and atomic force microscopy (AFM) combined with epifluorescence microscopy (EFM). Cells formed a monolayer biofilm and were preferably attached to the cracks/defects of pyrite surfaces. Biofilm and planktonic cells exhibited significant morphological differences. Capsular EPS were observed in both biofilm and planktonic cells.

1. Introduction

The mobilization of metal cations from often almost insoluble ores by biological oxidation and complexation processes is referred to as bioleaching (Rohwerder et al., 2003). The recovery of heavy metals such as zinc, cobalt, copper and nickel by an application of microorganisms is now a widely used technique (Rawlings and Johnson, 2007). Around 20% of copper production worldwide was done by biohydrometallurgical operations in 2010 (Schippers et al., 2013). However, bioleaching can occur spontaneously in nature and cause serious environmental problems like acid mine drainage (AMD) (Hallberg, 2010). There are many species of prokaryotes that have been reported in AMD and relevant environments (Johnson and Hallberg, 2003; Schippers et al., 2010). Acidophilic archaea belonging to *Thermoplasmatales* including *Thermoplamsa*, *Picrophilus*, *Ferroplasma* and *Acidiplasma* are the most common acidophiles of all known microorganisms.

Ferroplasma acidiphilum was first isolated from a semi-industrial bioleaching reactor processing arsenopyrite in Kazakhstan (Golyshina et al., 2000). *Ferroplasma* spp. are present in various acidic man-made operations such as leaching tanks/heaps and also natural habitats, which are considered as hostile environments. The family *Ferroplasmaceae* received scientific attention for its lifestyle in extremely acidic environments and new insights into acid and metal tolerance for cells without a protective cell wall. A key explanation for *Ferroplasma* spp. flourishing in acidic environments are their membrane lipids which are mainly composed of caldarchaetidylglycerol tetraether-linked monolayers (Macalady et al., 2004). *Ferroplasma* spp. are considered to be major players in global iron and sulfur cycling (Edwards et al., 2000; Golyshina, 2011).

Biofilms are communities of microorganisms attached to a surface embedded in extracellular polymeric substances (EPS). EPS mainly contain carbohydrates, proteins, lipids, nucleic acids and complexed metal ions (Flemming and Wingender, 2010). Attachment of microorganisms to mineral surfaces is of great importance for the process of mineral dissolution (Vera et al., 2013). Evidence showed that attachment of cells of *Acidithiobacillus ferrooxidans* to pyrite correlated with the degree of pyrite crystallization (Sanhueza et al., 1999). EPS mediate the contact between cells and metal sulfide (MS) and help to facilitate the dissolution of a MS due to ferric iron complexation, thus providing a reaction space for the chemical attack on a MS (Sand and Gehrke, 2006). EPS of *At. ferrooxidans* contain the carbohydrates glucose, rhamnose, fucose, xylose, mannose, C12–C20 saturated fatty acids, glucuronic acid, and Fe(III) ions (Gehrke et al., 1998). More than 80% of bacterial cells were attached to the non-limiting surfaces within 24 h, although less than 5% of the available surface area was colonized (Sand et al., 1998).

Archaeal biofilms are a common phenomenon and as complex as bacterial ones (Fröls, 2013; Orell et al., 2013). Some data have shown characteristics of attachment, biofilms and EPS composition of

* Corresponding author at: Universität Duisburg-Essen, Fakultät für Chemie, Biofilm Centre, Aquatic Biotechnology., Universitätsstr. 5, 45141 Essen, Germany. Tel.: +49 201 1837080; fax: +49 201 1837090.
E-mail address: mario.vera@uni-due.de (M. Vera).

http://dx.doi.org/10.1016/j.hydromet.2014.07.001
0304-386X/

Sulfolobus spp. (Koerdt et al., 2010, 2012). However, in these studies cells were grown with organic substrates and no applicable data are available for bioleaching processes. A biofilm of *Sulfolobus metallicus* was reported to develop on the support of a biotrickling filter during hydrogen sulfide/sulfur oxidation (Morales et al., 2011). A genome analysis indicated that several genes may be involved in adhesion and biofilm formation in *Metallosphaera sedula* (Auernik et al., 2008). Cells of *M. hakonensis* adhered to different MS and have maximum surface coverage at their optimal growth temperature. In addition, cells showed selective attachment to different sulfide minerals (Africa et al., 2013).

Although archaea are almost ubiquitously present in biomining ecosystems, very few investigations on acidophilic archaea for their role in bioleaching and AMD have been conducted (Brune and Bayer, 2012). In this study biofilm development of *F. acidiphilum* was examined in order to get an improved knowledge of the interaction of iron-oxidizing archaea and surfaces as well as colonization and growth on pyrite. Several microscopical techniques, including confocal laser scanning microscopy (CLSM), scanning electron microscopy (SEM) and atomic force microscopy (AFM) combined with epifluorescence microscopy (EFM) as well as the floating filter technique were used.

2. Materials and methods

2.1. Strain and cultivation

F. acidiphilum BRGM4 (DSM 28986) was isolated from a pilot-scale bioreactor (d'Hugues et al., 2008). 16S rRNA gene sequence analysis demonstrated that strain BRGM4 (GenBank accession no. KJ847278) showed sequence identity of 99% with the type strain *F. acidiphilum* Y (Golyshina et al., 2000). *F. acidiphilum* BRGM4 was cultivated in Mackintosh (MAC) medium (Mackintosh, 1978). Cells were grown at an initial pH of 1.7 in 5 L bottles containing 4 g/L iron (II) ions and 0.2 g/L yeast extract at 37 °C with agitation and aeration. For bioleaching, attachment and floating filter experiments, cells in late exponential phase were harvested by centrifugation at 8000 rpm for 15 min.

2.2. Pyrite preparation

Pyrite coupons with a size of approx. 1 cm × 1 cm × 2 mm were cut from cubes (origin Navajun, Spain). Grains with a size of 50–200 μm were selected after grinding and sieving. Both, slices and grains, were washed with boiling 6 M HCl for 30 min, rinsed with deionized water until neutral pH and three times with acetone. After cleaning, pyrite was dried at 80 °C for 12 h and sterilized for 24 h at 120 °C under a nitrogen atmosphere.

2.3. Leaching experiments

300-mL Erlenmeyer flasks containing 5 g of pyrite grains (50–100 μm grain sizes) and 100 mL of MAC medium (pH 1.7) and 0.2 g/L yeast extract were inoculated with *F. acidiphilum* BRGM4 at an initial cell number of 1.2×10^8 cells/mL. Abiotic controls were also done. Cell numbers were determined by direct microscopic counts and pH of the leachates was measured using a digital pH meter (Model pH 537, WTW). Iron ions were quantified using the phenanthroline method (according to DIN 38406-1).

2.4. Floating filter technique and CLSM

5×10^7 cells were filtered on autoclaved polycarbonate filters (GTTB, Ø 2.5 cm, 0.2 μm pore size, Millipore®) and immediately transferred to MAC medium containing 5 g/L iron (II) ions coupled with additional conditions. These included glucose supplementation (1 g/L) and P_i starvation (by incubation in MAC medium prepared without Pi). Cells grown on filters or pyrite were stained by 4′,6-diamidino-2-phenylindole (DAPI) or Sypro Red (Invitrogen). Polysaccharide moieties were observed by using the fluorescently labeled lectins Concanavalin A (Con A) or *Limulus polyphemus* agglutinin (LPA) (EY Laboratories), respectively. The staining of biofilms on filters was conducted as previously described (Bellenberg et al., 2012). A similar procedure was applied for pyrite samples, except that samples were stained in a coverwell chamber of 20 mm in diameter and 0.5 mm in depth (Invitrogen). Freshly-stained pyrite samples were visualized by CLSM using a TCS SP5X, controlled by the LASAF 2.4.1 build 6384 (Leica, Heidelberg, Germany). The system was equipped with an upright microscope and a super continuum light source (470–670 nm) as well as a 405 nm laser diode. Images were collected with a 63× water immersion lens with a numerical aperture (NA) of 1.2 and a 63× water immersible lens with a NA of 0.9. CLSM data sets were recorded in sequential mode in order to avoid interference of the fluorochrome emission signals between two different channels. Surface topography and texture of the pyrite surface were recorded by using CLSM in reflection mode.

2.5. AFM & EFM

Pyrite slices were rinsed with sterile MAC medium and deionized water. Cells attached on pyrite coupons and their EPS were stained by Syto 9 (Invitrogen) and fluorescently labeled Con A, respectively as mentioned in Section 2.4. Stained samples were dried at room temperature and visualized by EFM (Zeiss, Germany) combined with AFM (BioMaterial™Workstation, JPK Instruments) for the investigation of cell morphology and distribution on the surfaces of pyrite coupons as described previously (González et al., 2012; Mangold et al., 2008).

2.6. SEM observations

Pyrite slices incubated with cells were rinsed with deionized water and then successively dehydrated with increasing concentrations of acetone (60%, 80% and 90%) and stored overnight at 4 °C in 90% acetone. Samples were subjected to critical-point drying and coated with graphite and gold. Specimens were examined with a JEOL JSM-6330F microscope, FE-SEM at 10 kV.

3. Results and discussion

3.1. Effects of substrates on cell morphology

Comparative studies on the cell morphology of *F. acidiphilum*, grown on iron (II) sulfate and yeast extract with or without glucose over time, were performed. Cells showed morphological variability and thus responded to defined growth conditions. As shown in Fig. 1, young cultures (3 days, early exponential phase) grown on iron (II) sulfate were characterized by irregularly shaped spherical cells. In contrast, cells taken from early stationary phase cultures (7 days) were pleomorphic. A substantial proportion of cells showed extensions with a size of 0.3–0.4 μm. These occurred more abundant in cells taken from stationary phase cultures, as compared to those cells from exponential phase cultures. With the addition of glucose (1 g/L), cells appeared to be also pleomorphic and accumulated in chains containing several cells/buds (Fig. 1b). This preference to form aggregates was possibly due to an enhanced EPS production because of glucose supplementation. A similar phenomenon of increased EPS production has been observed in *At. ferrooxidans* after addition of glucose or galactose (Bellenberg et al., 2012). *F. acidiphilum* proliferates via budding (Golyshina et al., 2000). Buds were observed in both, planktonic and biofilm cells. Iron (II) sulfate grown cells in the exponential phase varied from 1.1 to 2.5 μm with bud sizes ranging from 0.3 to 0.6 μm, while cells in stationary phase were between 0.3 and 2.8 μm, with bud sizes ranging from 0.3 to 0.8 μm. Pyrite-attached cells showed morphological differences compared to planktonic cells (Fig. 2). They were slightly rod-shaped with an approximate size of 0.7 × 1.2 μm. *Ferroplasma*, *Acidiplasma* and *Thermoplasma*, unlike other archaeal genera, lack a cell wall (Albers

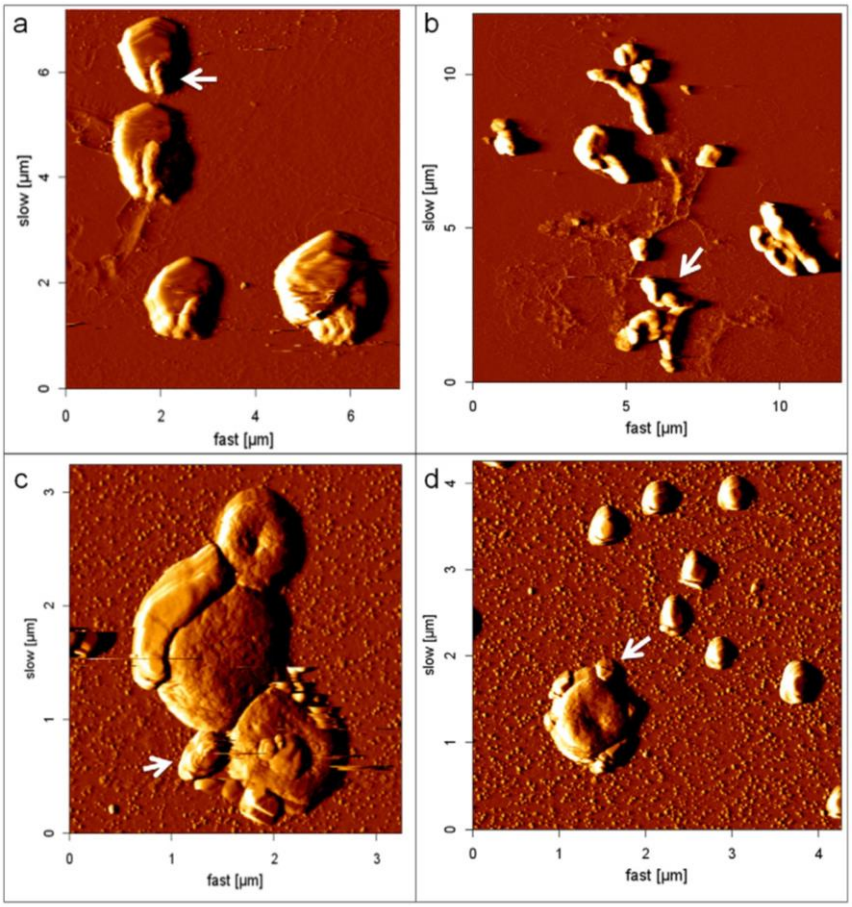

Fig. 1. Planktonic cells of *F. acidiphilum* grown on iron (II) ions visualized by AFM on glass (a, 3 days. b, 3 days, addition of glucose. c and d, 7 days). Arrows show cell buds.

and Meyer, 2011; Golyshina et al., 2009). Their cytoplasmic membrane is the only structural barrier against the surrounding environment. Consequently, environmental influences, such as variations in pH value and ion concentrations, directly affect the cell membrane. In addition, due to the fluidity of lipid membranes it is not surprising that cells of *F. acidiphilum* exhibit pleomorphy in planktonic state, when grown with different energy sources. Simultaneously, it is likely that biofilm cells displayed relatively homogeneous morphology on pyrite due to the support of the solid surface for maintenance of cell structures. Interferences on the AFM images were observed in the case of scanning cells from 7 days old cultures or cells grown with addition of glucose to the medium (Fig. 1b and c). These distortions are normally observed if high amounts of EPS are surrounding the cells (Mangold et al., 2008). This result seems to indicate that iron grown cells in the early stationary phase or with glucose supplementation produce more EPS than cells in early exponential phase. This finding also agrees with early reports that archaeal cells of *Haloferax* and *Sulfolobus* produce increased amounts of EPS over time (Antón et al., 1988; Nicolaus et al., 1993). EPS from cell-wall lacking archaea relevant to bioleaching have not been reported. N-glycosylation of surface proteins in acidophilic archaea is essential for these organisms to survive in the extremely acidic conditions. N-linked glycans and glycoproteins are key surface components of *T. acidophilum* (Vinogradov et al., 2012). *F. acidiphilum* BRGM4 might possess such functional groups (e.g. glycans) covalently attached to the proteinaceous layer or their membrane and the production of these extracellular components might be dependent on substrate availability. In addition, it has been shown that cell appendages (e.g. pili or flagella) are involved in *S. solfataricus* attachment to surfaces (Zolghadr et al., 2010). However, with the techniques applied we could not obtain clear evidences of the presence of similar cell appendages in *F. acidiphilum* BRGM4.

3.2. Bioleaching of pyrite

Strains of *Ferroplasma* have been shown to oxidize MS (e.g. pyrite or chalcopyrite) in pure culture (Okibe et al., 2003; Zhou et al., 2008) in the presence of trace amounts of yeast extract. Since cells of *F. acidiphilum* BRGM4 are not able to grow on 0.02% yeast extract as unique energy source (not shown), we tested growth on pyrite plus 0.02% yeast extract as energy source (Fig. 3). In the non-inoculated cultures (sterile control), around 0.06 g/L of total iron was measured at the end of the experiments (Fig. 3). Obviously, pyrite dissolution was accelerated by strain BRGM4. However, a low overall pyrite oxidation was observed, with 0.9 g/L of total iron ions released and a final pH of 1.2 after 45 days, although cell numbers reached 10^9 cells/mL. By comparison, cells of *F. acidiphilum* BRGM4 had approximately 20 or 29 times lower pyrite oxidation rates than the ones for the iron-oxidizing bacterium *Leptospirillum ferriphilum* (Florian et al., 2011; Zhang et al., 2010) or the thermoacidophilic archaeon *Acidianus* RZ1 (unpublished results), respectively. *Ferroplasma* spp. need to consume considerable metabolic resources in order to

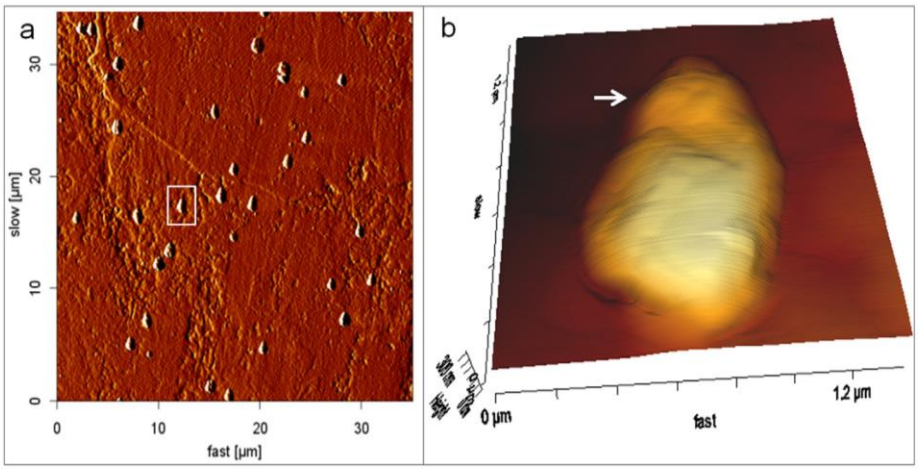

Fig. 2. Biofilm cells of *F. acidiphilum* on pyrite visualized using AFM (a, an overview of cells attached to pyrite; b, 3-D image of a single cell corresponding to the white frame in a). The arrow in (b) shows a cell bud.

survive in extremely acidic environments (Golyshina et al., 2006). The observed linear increase in cell numbers suggests that the attached cell population was actively dividing. As *F. acidiphilum* cannot oxidize the reduced inorganic sulfur compounds (RISCs), the planktonic cell subpopulation may have a reduced metabolic activity. However, this assumption needs further biochemical evidence.

Field emission SEM (FESEM) observations showed that the pyrite surfaces had rough areas and flat surfaces (Fig. S1). These rough surfaces are probably caused by the attack from ferric iron ions complexed in the EPS of *F. acidiphilum* BRGM4 cells and bulk solution. In contrast, the grains which appeared as not degraded by cells showed a relatively high light reflection by means of CLSM (not shown). Heterogeneous dissolution of pyrite by *At. ferrooxidans* was observed in the previous studies using SEM (Bennett and Tributsch, 1978; Edwards et al., 2001).

3.3. Biofilm formation on polycarbonate filters

Cells of *F. acidiphilum* grown on polycarbonate filters were visualized by CLSM combined with fluorescent probes for staining nucleic acids or glycoconjugates of their EPS. Cells were distributed relatively homogeneously on the filters (not shown) and were, due to the pore size, not able to penetrate through filters into the bulk solution. The spatial development of biofilm over time is shown in Fig. 4. The lectin Con A, recognizing ß-(1,3)-linked mannose and glucose residues of polysaccharides, was used to stain glycoconjugates as a major part of the EPS of *F. acidiphilum* BRGM4. After 1 day of incubation, cells showed Con A signal overlapping with DAPI signal. Thus, cells showed an EPS production at the early stage of biofilm formation, probably due to the contact with surfaces. Multilayered biofilms with a thickness of up to 20 µm were observed after 5 days of incubation. In contrast to the reports on *At. ferrooxidans* (Bellenberg et al., 2012), an enhancement of biofilm formation under Pi starvation was not observed (Fig. 4d). Mechanisms of response to Pi starvation have been described in *At. ferrooxidans* (Vera et al., 2003). As a canonical Pho regulon is absent in archaea, it is unclear how *Ferroplasma* spp. cells respond to Pi starvation. Interestingly, aggregates/microcolonies of approximately 20 µm in diameter were observed, when glucose was added (Fig. 4e). In the case of biofilms on filters, Con A signals were not only observed for the cells but also extended around the cells on the filters. In contrast, the Con A signal was restricted only to cell shapes of *F. acidiphilum* on pyrite surfaces (Figs. 2 and 6). This suggests that cells of *F. acidiphilum* are able to modify their biofilm formation and EPS production patterns in response to energy substrates. As CLSM

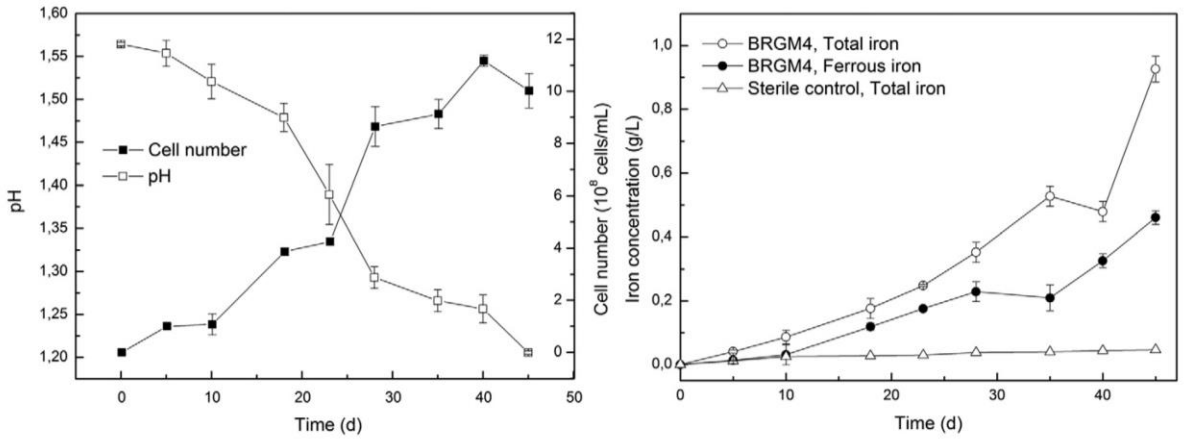

Fig. 3. Bioleaching of pyrite by cells of *F. acidiphilum*. Changes in pH and cell growth over time in flask cultures (left) and concentration of Fe(II) and Fe total dissolved over time (right). All measurements were performed in triplicate.

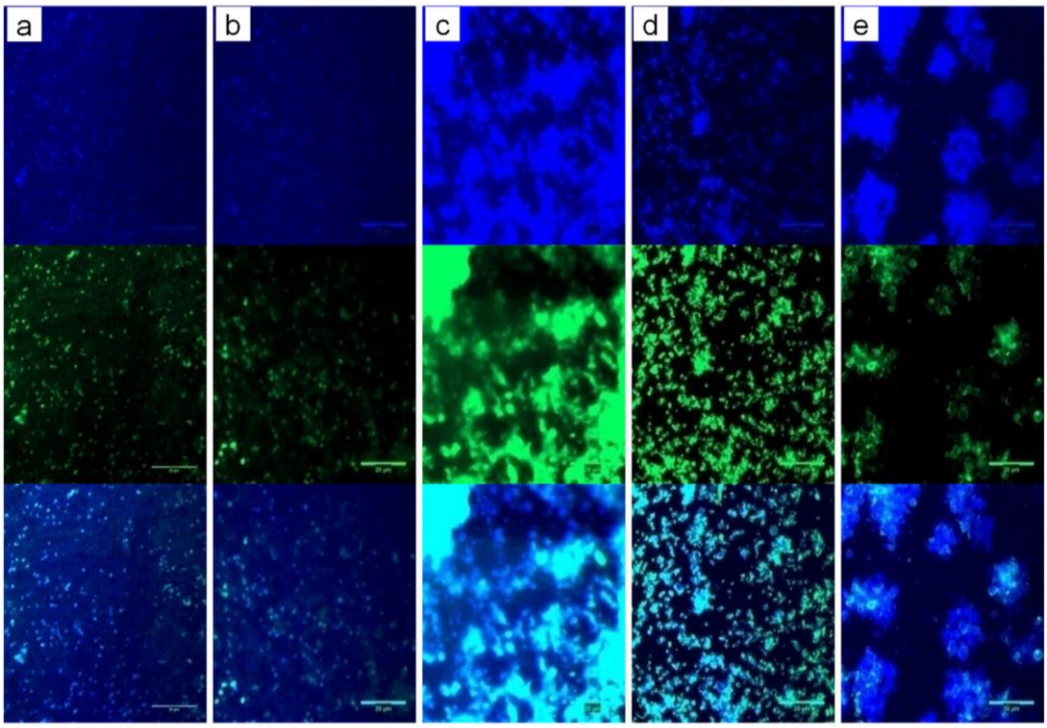

Fig. 4. Biofilms of *F. acidiphilum* on polycarbonate filters visualized by CLSM. In the upper and middle row of images, the signals from DAPI (blue) and Con A (green) are shown, while the images in the bottom row represent the merged images from both channels. Pictures a, b and c show cells after 1, 2 and 5 days of incubation on iron (II) sulfate. Cells grown under P_i starvation (d) and cells grown mixotrophically with glucose supplementation (1 g/L) (e) are shown. Bars represent 20 μm.

can collect 3 dimensional image series of a fully hydrated sample, information on the EPS production of cells at different locations becomes available (Neu et al., 2010). The upper layer of biofilm cells on floating filters showed a considerable reduced Con A signal compared to the ones in contact with the surface, as indicated in Fig. 5. Thus, it is apparent that cells synthesize more EPS when they are exposed to surfaces. Within the multilayered biofilms on polycarbonate filters or monolayered biofilms on pyrite, polymers containing mannose and glucose were present. *F. acidiphilum* was first described to be an obligately chemoautotrophic archaeon capable of oxidizing iron (II) ions. However, yeast extract and/or some vitamins are required for the cell growth. Later studies indicated that all *Ferroplasma* strains can grow heterotrophically, consequently they have to be considered as mixotrophs (Dopson et al., 2004). After several transfers to a medium with decreased iron (II) concentrations and increased sugar amounts we were able to obtain heterotrophically growing *F. acidiphilum* BRGM4 cultures. They utilized glucose as energy source and cell numbers reached 4×10^8 cells/mL in 8 days. In addition, cells were 2–3 times larger than iron (II) ion-grown ones (not

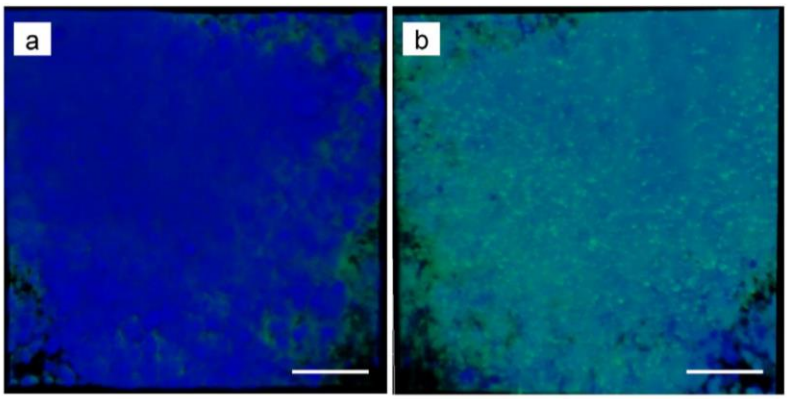

Fig. 5. CLSM images of biofilms of *F. acidiphilum* grown on iron (II) sulfate for 5 days on polycarbonate filters. Samples were stained by DAPI and fluorescently labeled Con A, respectively. Merged channels from both DAPI (blue) and Con A (green) are shown. (a) View from the upper layer biofilms facing air. (b) View from the underlayer biofilms in contact with polycarbonate surface. Bar represents 20 μm.

shown). There is evidence from *At. ferrooxidans* that glucose and galactose can be incorporated into capsular polysaccharides and cause an increased biofilm formation (Barreto et al., 2005; Bellenberg et al., 2012). In the case of cells of *F. acidiphilum* BRGM4, glucose may be used for the production of EPS to allow the cells to adsorb to polycarbonate surfaces. Bacteria produce diffusible extracellular signaling molecules, e.g., N-acylhomoserine lactones (AHLs) and oligopeptides, to monitor their own population density and to coordinate the expression of specific sets of genes in response to the cell density. The communication in biomining bacteria via AHLs is thought to be a widespread phenomenon and involved in cell-mineral interactions and biofilm formation (González et al., 2012; Ruiz et al., 2008). As expected, we did not detect any AHLs in pure culture of *F. acidiphilum* BRGM4 (not shown). This agrees with the previous findings in *F. acidarmanus* (Baker-Austin et al., 2010).

3.4. Attachment to and biofilm formation on pyrite

A combination of AFM and EFM has been used for visualization of surfaces with the advantage of high resolution and of identification of biological specimens (Mangold et al., 2008). As shown in Fig. 6, after attachment of cells to a pyrite surface a monolayer biofilm was formed. A similar behavior has been reported previously for acidophilic bacteria (Mangold et al., 2008; Noël et al., 2010). Biofilms formed by heterotrophic prokaryotes or phototrophs usually consist of dynamic, multilayer structures that can grow to three-dimensional macrocommunities (Stoodley et al., 2002). In contrast, leaching

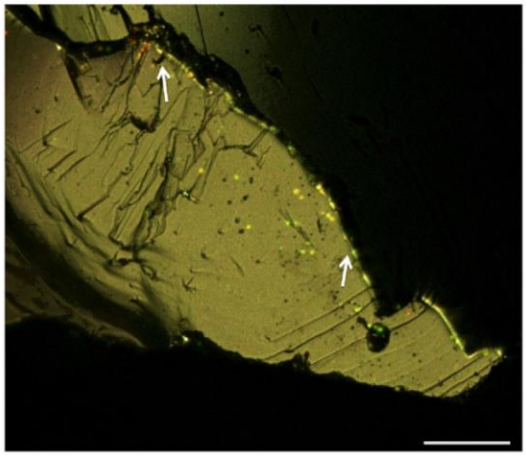

Fig. 7. CLSM image showing a maximum projection of a pyrite grain (200–500 mesh) colonized with cells of *F. acidiphilum* after 7 days of incubation. Cells were double stained with SyproRed (red) specific for proteins and fluorescent labeled LPA (green) specific for sialic acid residues in polysaccharides. Signals from both fluorescent channels plus light reflection (to image the pyrite grain surface) were recorded; the merged image from all three channels is shown. As indicated by arrows, the cell colonization pattern strongly correlates with surface imperfections/topographic defects. Bar represents 10 μm.

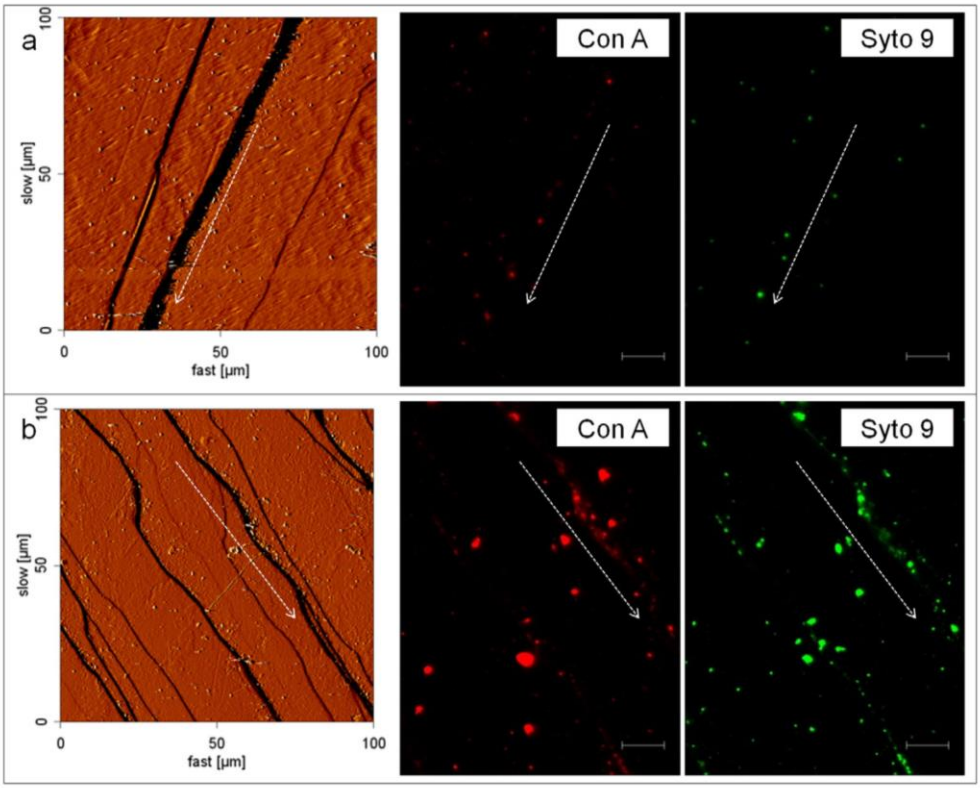

Fig. 6. Biofilm cells of *F. acidiphilum* on pyrite (a, 5 h and b, 7 days) visualized by AFM (left) and EFM (Con A and Syto 9 staining, right). Arrows show cell attachment to cracks or imperfections. Bars represent 10 μm.

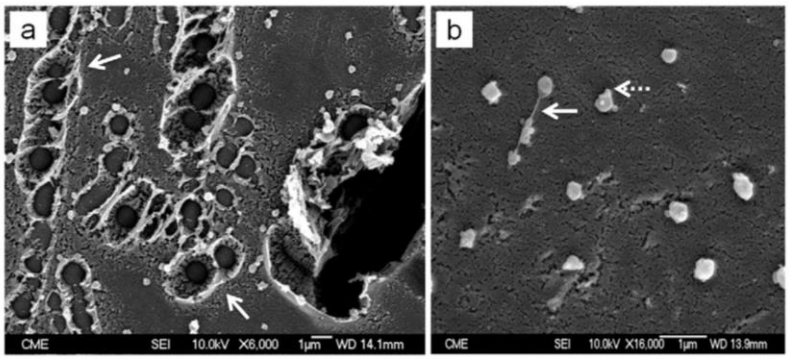

Fig. 8. SEM images of surfaces of a pyrite slice after 1 month of bioleaching with *F. acidiphilum*. Arrows in the left image (a) show isolated or connected pits. Arrows in the right image (b) show threads connecting cells (solid arrow) and cell buds (dash arrow), respectively.

microorganisms mainly develop monolayer biofilms on MS surfaces. These microbes attach to the surface of a MS in order to obtain energy by metabolizing compounds released during the dissolution of mineral substrates. Two distinct biofilm morphologies were described in *F. acidarmanus* Fer1: A multilayer film was formed on pyrite surfaces after 38 days and up to 5 mm-long filaments were found on the sintered glass spargers in the gas lift bioreactors (Baker-Austin et al., 2010). Thus, the attachment of *Ferroplasma* spp. to surfaces and the subsequent biofilm formation vary among the species, as described for other leaching bacteria (Ghauri et al., 2007).

Cells started colonizing pyrite within the first 5 h of incubation (Fig. 6a) and showed overlapping Syto 9 and Con A signals. This suggests that glycoconjugates were produced by the attached cells. Preferential attachment was observed along topographical faults/cracks of the pyrite surface (Fig. 6, arrows), a phenomenon also described for other leaching bacteria (Florian et al., 2010; Mangold et al., 2008; Noël et al., 2010). CLSM data of fully hydrated samples confirmed this phenomenon (Fig. 7). Obviously, large parts of the pyrite surfaces (≥80%) remained free of cells. Low coverage of pyrite with *F. acidiphilum* cells seems to be correlated to their limited pyrite leaching ability.

SEM was also applied to investigate the distribution of cells of *F. acidiphilum* on pyrite. As shown in Fig. 8, after 1 month of cultivation few cells were attached to pyrite. Extensive pits were found, which were heterogeneously distributed over the pyrite surface and often cell-shaped (1–2 μm in diameters). These pits were either isolated or connected to form long chains of pits. Similar dissolution patterns of pyrite have been reported in the previous studies (Edwards et al., 2001; Rodriguez-Leiva and Tributsch, 1988).

Biofilm formation and propagation occur by three different mechanisms: (1) the redistribution of surface-attached but motile cells, (2) the multiplication of attached cells and (3) attachment of cells from the bulk aqueous phase (Stoodley et al., 2002). Attached cells with buds were visible, as indicated in Fig. 8b (dash arrow). In addition, threads connecting cells, which probably correspond to shrunken EPS due to the dehydration during sample preparation (e.g. acetone treatment) were also evident (Fig. 8b, solid arrow). The production of EPS by *F. acidiphilum* BRGM4 was observed by fluorescent lectin-binding analysis (FLBA) and various glycoconjugates in biofilm cells were detected (unpublished data). The lectins showing a positive signal had specificities for e.g. mannose and glucose. These sugar monomers have been found also in EPS of other acidophilic bacteria (Gehrke et al., 1998; Harneit et al., 2006). In case of SEM observations, cells seem to appear slightly deformed and contracted to relatively small sizes (0.3–0.5 μm) (Fig. 8). Hence, various combined microscopical techniques are needed to reveal details of the complex interfacial interactions between archaeal cells and surfaces.

4. Conclusions

This study aimed at providing a better understanding of interfacial interactions between cells of the acidophilic archaeon *F. acidiphilum* and surfaces. Attachment and subsequent biofilm formation were investigated on polycarbonate and pyrite surfaces by various microscopical techniques. Cells of *F. acidiphilum* BRGM4 grew heterogeneously on filters over time and seem to modify their biofilms according to the substrate (e.g. glucose supplementation). EPS were evident in *F. acidiphilum* BRGM4 biofilms on pyrite and polycarbonate filters. Low coverage of the pyrite surface by cells seems to correlate with their low leaching ability. Bioleaching conducted by *F. acidiphilum* occurs possibly via combined contact and non-contact mechanisms.

Supplementary data to this article can be found online at http://dx.doi.org/10.1016/j.hydromet.2014.07.001.

Acknowledgments

We thank Prof. Dr. Barrie Johnson for providing *F. acidiphilum* BRGM4. R. Zhang appreciates China Scholarship Council for financial support (No. 2010637124).

References

Africa, C.J., van Hille, R.P., Sand, W., Harrison, S.T., 2013. Investigation and in situ visualisation of interfacial interactions of thermophilic microorganisms with metal-sulphides in a simulated heap environment. Miner. Eng. 48, 100–1017.
Albers, S.-V., Meyer, B.H., 2011. The archaeal cell envelope. Nat. Rev. Microbiol. 9, 414–426.
Antón, J., Meseguer, I., Rodriguez-Valera, F., 1988. Production of an extracellular polysaccharide by *Haloferax mediterranei*. Appl. Environ. Microbiol. 54, 2381–2386.
Auernik, K.S., Maezato, Y., Blum, P.H., Kelly, R.M., 2008. The genome sequence of the metal-mobilizing, extremely thermoacidophilic archaeon *Metallosphaera sedula* provides insights into bioleaching-associated metabolism. Appl. Environ. Microbiol. 74, 682–692.
Baker-Austin, C., Potrykus, J., Wexler, M., Bond, P.L., Dopson, M., 2010. Biofilm development in the extremely acidophilic archaeon '*Ferroplasma acidarmanus*' Fer1. Extremophiles 14, 485–491.
Barreto, M., Gehrke, T., Harneit, K., Sand, W., Jedlicki, E., Holmes, D., 2005. Unexpected insights into biofilm formation by *Acidithiobacillus ferrooxidans* revealed by genome analysis and experimental approaches. In: Harrison, S.T.L., Rawlings, D.E., Petersen, J. (Eds.), Proceedings of the 16th International Biohydrometallurgy Symposium. Compress, Cape Town, South Africa, pp. 25–29.
Bellenberg, S., Leon-Morales, C.F., Sand, W., Vera, M., 2012. Visualization of capsular polysaccharide induction in *Acidithiobacillus ferrooxidans*. Hydrometallurgy 129–130, 82–89.
Bennett, J., Tributsch, H., 1978. Bacterial leaching patterns on pyrite crystal surfaces. J. Bacteriol. 134, 310–317.
Brune, K.D., Bayer, T.S., 2012. Engineering microbial consortia to enhance biomining and bioremediation. Front. Microbiol. 3, 203.
d'Hugues, P., Joulian, C., Spolaore, P., Michel, C., Garrido, F., Morin, D., 2008. Continuous bioleaching of a pyrite concentrate in stirred reactors: population dynamics and exopolysaccharide production vs. bioleaching performance. Hydrometallurgy 94, 34–41.

Dopson, M., Baker-Austin, C., Hind, A., Bowman, J.P., Bond, P.L., 2004. Characterization of *Ferroplasma* isolates and *Ferroplasma acidarmanus* sp. nov., extreme acidophiles from acid mine drainage and industrial bioleaching environments. Appl. Environ. Microbiol. 70, 2079–2088.

Edwards, K.J., Bond, P.L., Gihring, T.M., Banfield, J.F., 2000. An archaeal iron-oxidizing extreme acidophile important in acid mine drainage. Science 287, 1796–1799.

Edwards, K.J., Hu, B., Hamers, R.J., Banfield, J.F., 2001. A new look at microbial leaching patterns on sulfide minerals. FEMS Microbiol. Ecol. 34, 197–206.

Flemming, H.C., Wingender, J., 2010. The biofilm matrix. Nat. Rev. Microbiol. 8, 623–633.

Florian, B., Noël, N., Sand, W., 2010. Visualization of initial attachment of bioleaching bacteria using combined atomic force and epifluorescence microscopy. Miner. Eng. 23, 532–535.

Florian, B., Noël, N., Thyssen, C., Felschau, I., Sand, W., 2011. Some quantitative data on bacterial attachment to pyrite. Miner. Eng. 24, 1132–1138.

Frӧls, S., 2013. Archaeal biofilms: widespread and complex. Biochem. Soc. Trans. 41, 393–398.

Gehrke, T., Telegdi, J., Thierry, D., Sand, W., 1998. Importance of extracellular polymeric substances from *Thiobacillus ferrooxidans* for bioleaching. Appl. Environ. Microbiol. 64, 2743–2747.

Ghauri, M.A., Okibe, N., Johnson, D.B., 2007. Attachment of acidophilic bacteria to solid surfaces: the significance of species and strain variations. Hydrometallurgy 85, 72–80.

Golyshina, O.V., 2011. Environmental, biogeographic, and biochemical patterns of archaea of the family *Ferroplasmaceae*. Appl. Environ. Microbiol. 77, 5071–5078.

Golyshina, O.V., Pivovarova, T.A., Karavaiko, G.I., Kondratéva, T.F., Moore, E., Abraham, W.-R., Lünsdorf, H., Timmis, K.N., Yakimov, M.M., Golyshin, P., 2000. *Ferroplasma acidiphilum* gen. nov., sp. nov., an acidophilic, autotrophic, ferrous-iron-oxidizing, cell-wall-lacking, mesophilic member of the *Ferroplasmaceae* fam. nov., comprising a distinct lineage of the Archaea. Int. J. Syst. Evol. Microbiol. 50, 997–1006.

Golyshina, O.V., Golyshin, P.N., Timmis, K.N., Ferrer, M., 2006. The 'pH optimum anomaly' of intracellular enzymes of *Ferroplasma acidiphilum*. Environ. Microbiol. 8, 416–425.

Golyshina, O.V., Yakimov, M.M., Lünsdorf, H., Ferrer, M., Nimtz, M., Timmis, K.N., Wray, V., Tindall, B.J., Golyshin, P.N., 2009. *Acidiplasma aeolicum* gen. nov., sp. nov., a euryarchaeon of the family *Ferroplasmaceae* isolated from a hydrothermal pool, and transfer of *Ferroplasma cupricumulans* to *Acidiplasma cupricumulans* comb. nov. Int. J. Syst. Evol. Microbiol. 59, 2815–2823.

González, A., Bellenberg, S., Mamani, S., Ruiz, L., Echeverría, A., Soulère, L., Doutheau, A., Demergasso, C., Sand, W., Queneau, Y., 2012. AHL signaling molecules with a large acyl chain enhance biofilm formation on sulfur and metal sulfides by the bioleaching bacterium *Acidithiobacillus ferrooxidans*. Appl. Microbiol. Biotechnol. 97, 3729–3737.

Hallberg, K., 2010. New perspectives in acid mine drainage microbiology. Hydrometallurgy 104, 448–453.

Harneit, K., Göksel, A., Kock, D., Klock, J.H., Gehrke, T., Sand, W., 2006. Adhesion to metal sulfide surfaces by cells of *Acidithiobacillus ferrooxidans*, *Acidithiobacillus thiooxidans* and *Leptospirillum ferrooxidans*. Hydrometallurgy 83, 245–254.

Johnson, D.B., Hallberg, K.B., 2003. The microbiology of acidic mine waters. Res. Microbiol. 154, 466–473.

Koerdt, A., Gödeke, J., Berger, J., Thormann, K.M., Albers, S.V., 2010. Crenarchaeal biofilm formation under extreme conditions. PLoS ONE 5 (11), e14104. http://dx.doi.org/10.1371/journal.pone.0014104.e14104.

Koerdt, A., Jachlewski, S., Ghosh, A., Wingender, J., Siebers, B., Albers, S.V., 2012. Complementation of *Sulfolobus solfataricus* PBL2025 with an α-mannosidase: effects on surface attachment and biofilm formation. Extremophiles 16, 115–125.

Macalady, J.L., Vestling, M.M., Baumler, D., Boekelheide, N., Kaspar, C.W., Banfield, J.F., 2004. Tetraether-linked membrane monolayers in *Ferroplasma* spp: a key to survival in acid. Extremophiles 8, 411–419.

Mackintosh, M.E., 1978. Nitrogen fixation by *Thiobacillus ferrooxidans*. J. Gen. Microbiol. 105, 215–218.

Mangold, S., Harneit, K., Rohwerder, T., Claus, G., Sand, W., 2008. Novel combination of atomic force microscopy and epifluorescence microscopy for visualization of leaching bacteria on pyrite. Appl. Environ. Microbiol. 74, 410–415.

Morales, M., Arancibia, J., Lemus, M., Silva, J., Gentina, J.C., Aroca, G., 2011. Bio-oxidation of H_2S by *Sulfolobus metallicus*. Biotechnol. Lett. 33, 2141–2145.

Neu, T.R., Manz, B., Volke, F., Dynes, J.J., Hitchcock, A.P., Lawrence, J.R., 2010. Advanced imaging techniques for assessment of structure, composition and function in biofilm systems. FEMS Microbiol. Ecol. 72, 1–21.

Nicolaus, B., Manca, M.C., Ramano, I., Lama, L., 1993. Production of an exopolysaccharide from two thermophilic archaea belonging to the genus *Sulfolobus*. FEMS Microbiol. Lett. 109, 203–206.

Noël, N., Florian, B., Sand, W., 2010. AFM & EFM study on attachment of acidophilic leaching organisms. Hydrometallurgy 104, 370–375.

Okibe, N., Gericke, M., Hallberg, K.B., Johnson, D.B., 2003. Enumeration and characterization of acidophilic microorganisms isolated from a pilot plant stirred-tank bioleaching operation. Appl. Environ. Microbiol. 69, 1936–1943.

Orell, A., Frӧls, S., Albers, S.V., 2013. Archaeal biofilms: the great unexplored. Annu. Rev. Microbiol. 67, 337–354.

Rawlings, D.E., Johnson, D.B., 2007. The microbiology of biomining: development and optimization of mineral-oxidizing microbial consortia. Microbiology 153, 315–324.

Rodriguez-Leiva, M., Tributsch, H., 1988. Morphology of bacterial leaching patterns by *Thiobacillus ferrooxidans* on synthetic pyrite. Arch. Microbiol. 149, 401–405.

Rohwerder, T., Gehrke, T., Kinzler, K., Sand, W., 2003. Bioleaching review part A. Appl. Microbiol. Biotechnol. 63, 239–248.

Ruiz, L.M., Valenzuela, S., Castro, M., Gonzalez, A., Frezza, M., Soulère, L., Rohwerder, T., Queneau, Y., Doutheau, A., Sand, W., 2008. AHL communication is a widespread phenomenon in biomining bacteria and seems to be involved in mineral-adhesion efficiency. Hydrometallurgy 94, 133–137.

Sand, W., Gehrke, T., 2006. Extracellular polymeric substances mediate bioleaching/biocorrosion via interfacial processes involving iron (III) ions and acidophilic bacteria. Res. Microbiol. 157, 49–56.

Sand, W., Gehrke, T., Hallmann, R., Schippers, A., 1998. Towards a novel bioleaching mechanism. Min. Pro. Ext. Met. Rev. 19, 97–106.

Sanhueza, A., Ferrer, I., Vargas, T., Amils, R., Sánchez, C., 1999. Attachment of *Thiobacillus ferrooxidans* on synthetic pyrite of varying structural and electronic properties. Hydrometallurgy 51, 115–129.

Schippers, A., Breuker, A., Blazejak, A., Bosecker, K., Kock, D., Wright, T., 2010. The biogeochemistry and microbiology of sulfidic mine waste and bioleaching dumps and heaps, and novel Fe(II)-oxidizing bacteria. Hydrometallurgy 104, 342–350.

Schippers, A., Hedrich, S., Vasters, J., Drobe, M., Sand, W., Willscher, S., 2013. Biomining: metal recovery from ores with microorganisms. In: Schippers, A., Glombitza, F., Sand, W. (Eds.), Advances in Biochemical Engineering/Biotechnology. Geobiotechnology Springer, Berlin. http://dx.doi.org/10.1007/10_2013_216.

Stoodley, P., Sauer, K., Davies, D., Costerton, J.W., 2002. Biofilms as complex differentiated communities. Annu. Rev. Microbiol. 56, 187–209.

Vera, M., Guiliani, N., Jerez, C.A., 2003. Proteomic and genomic analysis of the phosphate starvation response of *Acidithiobacillus ferrooxidans*. Hydrometallurgy 71, 125–132.

Vera, M., Schippers, A., Sand, W., 2013. Progress in bioleaching: fundamentals and mechanisms of bacterial metal sulfide oxidation—part A. Appl. Microbiol. Biotechnol. 97, 7529–7541.

Vinogradov, E., Deschatelets, L., Lamoureux, M., Patel, G.B., Tremblay, T.-L., Robotham, A., Goneau, M.-F., Cummings-Lorbetskie, C., Watson, D.C., Brisson, J.-R., 2012. Cell surface glycoproteins from *Thermoplasma acidophilum* are modified with an N-linked glycan containing 6-C-sulfofucose. Glycobiology 22, 1256–1267.

Zhang, R.Y., Xia, J.L., Peng, J.H., Zhang, Q., Zhang, C.G., Nie, Z.Y., Qiu, G.Z., 2010. A new strain *Leptospirillum ferriphilum* YTW315 for bioleaching of metal sulfides ores. T. Nonferr. Metal. Soc. 20, 135–141.

Zhou, H., Zhang, R., Hu, P., Zeng, W., Xie, Y., Wu, C., Qiu, G., 2008. Isolation and characterization of *Ferroplasma thermophilum* sp. nov., a novel extremely acidophilic, moderately thermophilic archaeon and its role in bioleaching of chalcopyrite. J. Appl. Microbiol. 105, 591–601.

Zolghadr, B., Klingl, A., Koerdt, A., Driessen, A.J., Rachel, R., Albers, S.-V., 2010. Appendage-mediated surface adherence of *Sulfolobus solfataricus*. J. Bacteriol. 192, 104–110.

Supplementary data

Fig. S1 SEM of *F. acidiphilum* cells on pyrite grains after 14 days of bioleaching (1, flat surfaces. 2, crude surfaces). Arrows show cells attached to surfaces.